Genetics: Early Online, published on November 16, 2017 as 10.1534/genetics.117.1119

# Elucidation of the two H3K36me3 histone methyltransferases Set2 and Ash1 in *Fusarium fujikuroi* unravels their different chromosomal targets and a major impact of Ash1 on genome stability

Slavica Janevska[1], Leonie Baumann[1], Christian M. K. Sieber[2], Martin Münsterkötter[3], Jonas Ulrich[4], Jörg Kämper[4], Ulrich Güldener[5], Bettina Tudzynski[1*]

[1] Institute of Plant Biology and Biotechnology, Westfälische Wilhelms-Universität Münster, Schlossplatz 8, 48143 Münster, Germany

[2] Department of Energy Joint Genome Institute, 2800 Mitchell Drive, Walnut Creek, CA 94598, USA

[3] Institute of Bioinformatics and Systems Biology, Helmholtz Zentrum München, Ingolstädter Landstraße 1, 85764 Oberschleißheim, Germany

[4] Institute for Applied Biosciences, Karlsruhe Institute of Technology, Fritz-Haber-Weg 4, 76131 Karlsruhe, Germany

[5] Chair of Genome-oriented Bioinformatics, TUM School of Life Sciences Weihenstephan, Technical University of Munich, Maximus-von-Imhof-Forum 3, 85354 Freising, Germany

* Corresponding author: Prof. Dr. Bettina Tudzynski, e-mail: tudzynsb@uni-muenster.de

Short title: Two H3K36 methyltransferases in *F. fujikuroi*

Keywords: *Fusarium fujikuroi*; Histone methyltransferase; H3K36me3; Genome stability; Secondary metabolism

## Abstract

In this work, we present a comprehensive analysis of the H3K36 histone methyltransferases Set2 and Ash1 in the filamentous ascomycete *Fusarium fujikuroi*. In *Saccharomyces cerevisiae*, one single methyltransferase, Set2, confers all H3K36 methylation, while there are two members of the Set2 family in filamentous fungi, and even more H3K36 methyltransferases in higher eukaryotes. Whereas the yeast Set2 homolog has been analyzed in fungi previously, the second member of the Set2 family, designated Ash1, has not been described for any filamentous fungus. Western blot and ChIP-Seq analyses confirmed that *F. fujikuroi* Set2 and Ash1 are H3K36-specific histone methyltransferases that deposit H3K36me3 at specific loci: Set2 is most likely responsible for H3K36 methylation of euchromatic regions of the genome, while Ash1 methylates H3K36 at the subtelomeric regions (facultative heterochromatin) of all chromosomes including the accessory chromosome XII. Our data indicate that H3K36me3 cannot be considered a hallmark of euchromatin in *F. fujikuroi*, and likely also other filamentous fungi, making them different to what is known about nuclear characteristics in yeast and higher eukaryotes. We suggest that the H3K36 methylation mark exerts specific functions when deposited at euchromatic or subtelomeric regions by Set2 or Ash1, respectively. We found an enhanced level of H3K27me3, an increased instability of subtelomeric regions and losses of the accessory chromosome XII over time in Δ*ash1* mutants, indicating an involvement of Ash1 in DNA repair processes. Further phenotypic analyses revealed a role of H3K36 methylation in vegetative growth, sporulation, secondary metabolite biosynthesis and virulence in *F. fujikuroi*.

# Introduction

The phytopathogenic ascomycete *Fusarium fujikuroi* is the founding member of the *Fusarium* (*Gibberella*) *fujikuroi* species complex (Leslie and Summerell 2006; Nirenberg and O'Donnell 1998) and the causative agent of the *bakanae* ("foolish seedling") disease of rice plants (Sun and Snyder 1981). Disease symptoms are induced due to the secretion of gibberellic acids (GAs) by *F. fujikuroi*, a group of highly bioactive and growth-promoting plant hormones. Infection of the rice roots results in the chlorotic hyper-elongation of rice internodes and finally, plant death (Bömke and Tudzynski 2009; Wiemann *et al*. 2013). Besides GAs, *F. fujikuroi* also produces a spectrum of other secondary metabolites (SMs), which are by definition not required for the general growth of the fungus, but are likely of benefit to the pathogen under mainly unknown conditions (Fox and Howlett 2008). The biosynthesis and regulation of some of them, *e.g.* of the two red pigments bikaverin (BIK) and fusarubins (FSR), as well as of the mycotoxins fusarins (FUS) and fusaric acid (FSA) have been well studied. On a molecular level, BIK and FSR are polyketide synthase (PKS)-derived products, FUS is condensed by a PKS-non-ribosomal peptide synthetase (NRPS) hybrid enzyme, while FSA biosynthesis requires two separate key enzymes, a PKS and an NRPS (Niehaus *et al*. 2013; Niehaus *et al*. 2014; Studt *et al*. 2012; Studt *et al*. 2016b; Wiemann *et al*. 2009).

While BIK, FSR and FSA gene clusters encode pathway-specific transcription factors (TFs) (Studt *et al*. 2012; Studt *et al*. 2016b; Wiemann *et al*. 2009), GA and FUS clusters do not (Niehaus *et al*. 2013; Tudzynski and Hölter 1998). In this regard, we are especially interested in global regulators and epigenetic regulation mechanisms that affect SM biosynthesis. Furthermore, a large number of putative SM gene clusters is not expressed under standard laboratory conditions in *F. fujikuroi* (and other fungi) (Wiemann *et al*. 2013), so that especially the perturbation of chromatin-mediated regulation represents a powerful tool for the upregulation of a greater set of genes.

The genome-wide and local regulation of gene expression through the covalent, yet reversible, post-translational modification of histone (H) proteins is well established in the literature, *e.g.* through the acetylation, methylation and phosphorylation of conserved lysine (K), arginine, serine and/or threonine residues (Brosch *et al*. 2008). The methylation of H3K9 and H3K27 is generally associated with gene silencing, and these marks are mainly found in stretches of constitutive and facultative heterochromatin, respectively (Rando and Chang 2009; Wiles and Selker 2017). In contrast, the methylation of H3K4 and H3K36 is generally described to be hallmarks of euchromatic regions with actively transcribed genes (Rando and Chang 2009; Wagner and Carpenter 2012).

In *Saccharomyces cerevisiae*, Set2 is the only histone methyltransferase dedicated to the mono-, di- and trimethylation (me1, me2, me3) of H3K36 (Strahl *et al*. 2002), while there are eight H3K36-specific methyltransferases homologous to *S. cerevisiae* Set2 in humans (Wagner and Carpenter 2012). Additionally, a Set2 homolog has been confirmed as H3K36-specific methyltransferase in the filamentous ascomycetous fungi *Neurospora crassa* and *Fusarium verticillioides* (Adhvaryu *et al*. 2005; Gu *et al*. 2017). Set2 is characterized by its catalytic Su(var)3-9, Enhancer-of-zeste, Trithorax (SET) domain that is essential for methyltransferase activity (Strahl *et al*. 2002). This is true for other SET domain-containing methyltransferases that have also been studied in filamentous fungi, *i.e.* Set1 (H3K4), Dim5/ClrD (H3K9) and Kmt6 (H3K27) (Connolly *et al*. 2013; Liu *et al*. 2015; Reyes-Dominguez *et al*. 2010; Studt *et al*. 2016a; Tamaru and Selker 2001).

*S. cerevisiae* Set2 has been shown to directly interact with the hyper-phosphorylated form of RNA polymerase II, depositing its H3K36me3 within gene bodies of actively transcribed genes during elongation (Kizer *et al*. 2005; Krogan *et al*. 2003), a mechanism which is conserved also in humans (Li *et al*. 2005; Sun *et al*. 2005). Furthermore, the trimethylation of H3K36 by *S. cerevisiae* Set2 within the body of a gene results in histone deacetylation *via* recruitment of the Reduced potassium dependency 3 small (Rpd3S) complex and

subsequently, in the prevention of aberrant transcriptional initiation within coding sequences (Carrozza *et al*. 2005; Keogh *et al*. 2005). In higher eukaryotes, mainly studied in *Drosophila melanogaster* and mammalian cells, this mark has been implicated in a number of vital cellular processes, such as alternative splicing, DNA replication and repair as well as the transfer of gene expression memory on to progeny, qualifying H3K36 methylation as a true epigenetic mark. Therefore, it is not surprising that the perturbation of this mark is associated with a range of human diseases, including cancer (Venkatesh and Workman 2013; Wagner and Carpenter 2012).

As a counterpart, H3K36-specific demethylases, *e.g.* the *S. cerevisiae* Jumonji C (JmjC) domain-containing demethylases Jdh1 and Rph1, have been reported to remove H3K36me2/me1 and H3K36me3/me2 marks, respectively (Kim and Buratowski 2007; Klose *et al*. 2007; Tsukada *et al*. 2006). In mammalian systems, the JHDM3/JMJD2 family of histone demethylases also counteracts H3K9 in addition to H3K36 methylation (Klose *et al*. 2006). Interestingly, this trait is conserved for yeast Rph1 which belongs to this protein family, although the H3K9me3 mark itself is not present in *S. cerevisiae* (Klose *et al*. 2007). The *Aspergillus nidulans* Rph1 homolog, designated Lysine demethylase A (KdmA), has been confirmed to be an H3K36me3 demethylase (Gacek-Matthews *et al*. 2015).

In this work, we present the identification of two H3K36-specific methyltransferases in *F. fujikuroi*, Set2 and Ash1, which deposit H3K36me3 at specific loci, at euchromatic and subtelomeric regions, respectively. Therefore, we suggest that H3K36me3 cannot be considered a hallmark of actively transcribed euchromatin in *F. fujikuroi*, and the same probably applies to other filamentous fungi. Chromatin immunoprecipitation with subsequent sequencing (ChIP-Seq) revealed that Ash1 deposits H3K36me3 at subtelomeres and at the accessory chromosome XII. We demonstrate that Ash1 contributes to chromosome stability, indicating a role of Ash1 in the repair of DNA double strand breaks. Furthermore, a detailed phenotypic analysis of Δ*set2* and Δa*sh1* mutants revealed an effect of both methyltransferases

on SM biosynthesis and pathogenicity. As a counterpart to the H3K36 methyltransferases, the Rph1/KdmA homolog Kdm4 was identified and functionally characterized in *F. fujikuroi*.

## Materials and Methods

### Fungal strains, media and growth conditions

*F. fujikuroi* IMI58289 (Commonwealth Mycological Institute, Kew, UK) (Wiemann *et al*. 2013) was used as parental wild-type (WT) strain for the generation of deletion, point-mutation and overexpression mutants. Plate assays were done in triplicates on solid V8 (30 mM $CaCO_3$, 20%, v/v, vegetable juice; Campbell Food, Puurs, Belgium), CM (Pontecorvo *et al*. 1953) and CD (Czapek Dox; Sigma-Aldrich, Steinheim, Germany) media, supplemented with 0-40 mM $H_2O_2$ if needed, and incubated for 7 days in darkness (28 °C), constant light (20 °C) or in the presence of a 12 h light/12 h dark cycle (LD; 18 °C). Production of conidia was assessed after growth on solid V8 medium for 14 days (LD; 18 °C). Prior to DNA isolation, the strains were grown on solid CM medium covered with a layer of cellophane for 3 days at 28 °C in the dark. Cultivation in liquid culture began with a pre-culture consisting of 100 mL Darken medium (Darken *et al*. 1959) in 300 mL-Erlenmeyer flasks, shaken for 3 days at 180 rpm and 28 °C in the dark. 0.5% (v/v) of the pre-culture was then transferred to the main culture, consisting of 100 mL ICI medium (Imperial Chemical Industries Ltd., London, UK) (Geissman *et al*. 1966) with 6 mM (N-) or 60 mM (N+) glutamine as sole nitrogen source. Cultivation continued for 3 or 7 days, for ChIP-Seq, microarray or SM analyses, respectively, under the conditions described above. For protoplast transformation of *F. fujikuroi*, 0.5% (v/v) of the pre-culture was transferred to 100 mL ICI medium, containing 10 g/L fructose instead of glucose and 0.5 g/L $(NH_4)_2SO_4$ as nitrogen source, and grown for no longer than 16 h.

## Plasmid constructions

The cloning of deletion, point-mutation, complementation and overexpression vectors was achieved through yeast recombinational cloning (Colot *et al*. 2006; Schumacher 2012). For the generation of gene deletion vectors, ca. 1 kb large upstream (5') and downstream (3') sequences of the genes of interest were amplified using primer pairs 5F/5R and 3F/3R, respectively (Table S1). The resistance cassette *hphR* (hygromycin B phosphotransferase gene under the control of the *PtrpC* promoter from *A. nidulans*) was amplified with hph_F/hph_R (Table S1) from the template pCSN44 (Staben *et al*. 1989), while *natR* (nourseothricin resistance gene including *A. nidulans PtrpC*) as amplified from the template pZPnat1 (GenBank AY631958). The yeast strain *S. cerevisiae* FY834 (Winston *et al*. 1995) was transformed with the obtained fragments as well as with the *Eco*RI/*Xho*I digested shuttle vector pRS426 (Christianson *et al*. 1992), yielding the deletion vectors p∆*set2*::*hphR*, p∆*ash1*::*hphR*, p∆*ash1*::*natR*, p∆*kdm4*::*hphR*.

For the generation of the p*H3K36A* point-mutation (Figure S1A) and p$H3K36A^{C}$ complementation (Figure S1B) vectors, *H3* (*FFUJ_09749*) including its 5' sequence was amplified in two fragments to insert the point-mutation (H3_mut_1F/H3_mut_K36A_1R; H3_mut_K36A_2F/H3_mut_2R; Table S2) or was amplified in one fragment (H3_mut_1F/H3_mut_2R; Table S2), respectively. Furthermore, the *H3* 3' sequence was amplified with H3_mut_3F/H3_mut_3R (Table S2). The resistance cassettes *hphR* and *natR* were generated as described above for p*H3K36A* and p$H3K36A^{C}$, respectively. *S. cerevisiae* FY834 was then transformed with the respective fragments as well as with the *Eco*RI/*Xho*I digested vector pRS426. Similarly, also p$SET2^{C}$ (Figure S2A), p$ASH1^{C}$ and p$ASH1^{H537K}$ (Figure S2B) were gained. Thus, the full-length *SET2* gene including its 5' sequence (set2_5F/set2_c_1R; set2_c_2F/set2_c_2R), the full-length *ASH1* gene including its 5' sequence (ash1_5F/ash1_c_1R; ash1_c_2F/ash1_c_2R) and the point-mutated version of

*ASH1* including its 5' sequence (ash1_5F/ash1_5R; ash1_mut_1F/ash1_mut_1R; ash1_mut_2F/ash1_c_2R) were amplified with primers found in Table S2. 3' sequences of *SET2* and *ASH1* as well as *natR* were gained as described above, and the respective fragments were cloned into *Eco*RI/*Xho*I digested pRS426. For the constitutive overexpression of *KDM4* *via* the *A. nidulans PoliC* promoter, the first 1.6 kb of *KDM4* were generated with OE_kdm4_F/OE_kdm4_R (Table S2) and fused to *Nco*I/*Not*I restricted vector pNDH-OGG (Schumacher. 2012), yielding pOE::*KDM4* (Figure S3C). The correct assembly of all point-mutation, complementation and overexpression vectors was verified by sequencing with primers listed in Table S2.

**Fungal transformations and analysis of transformants**

The transformation of *F. fujikuroi* protoplasts was performed as previously described (Tudzynski *et al*. 1999). Deletion cassettes were amplified from the p∆*set2*::*hphR*, p∆*ash1*::*hphR*, p∆*ash1*::*natR* or p∆*kdm4*::*hphR* vectors with primers 5F/3R (Table S1) and used for transformation. Furthermore, 10-40 µg of the *Pvu*II/*Xba*I digested p*H3K36A* (Figure S1A), the *Pvu*II/*Xba*I digested p$H3K36A^{C}$ (Figure S1B), the *Pvu*II linearized p$SET2^{C}$ (Figure S2A), the *Sca*I digested p$ASH1^{C}$ or p$ASH1^{H537K}$ (Figure S2B) or the circular pOE::*KDM4* (Figure S3C) vectors was applied. Gained transformants were selected using 100 µg/mL hygromycin B (Calbiochem, Darmstadt, Germany) or 100 µg/mL nourseothricin (Werner-Bioagents, Jena, Germany) resistance markers.

The homologous integration of resistance cassettes and the absence of WT genes were shown by Southern blot analysis and/or diagnostic polymerase chain reaction (PCR). Therefore, diagnostic PCRs for five independent deletion mutants of ∆*set2*, six deletion mutants of ∆*ash1*, six double deletion mutants of ∆*set2*/∆*ash1* (*ASH1* deletion in ∆*set2* T2), as well as three deletion mutants of ∆*kdm4* are depicted in Figures S4A, S5A and S6A/B. Furthermore, the correct recombination of 5' and 3' flanks and the absence of untransformed

nuclei was verified for five independent *H3K36A* mutants (Figure S1C), one *H3K36A*$^{C}$ mutant (Figure S1D), two *SET2*$^{C}$ mutants (Figure S2C) as well as three *ASH1*$^{C}$ and three *ASH1*$^{H537K}$ mutants (Figure S2D). The correct *in loco* integration of pOE::*KDM4* in three independent OE::*KDM4* mutants was shown when grown on CM with hygromycin B (Figure S3D). For the complemented transformants, it was confirmed that they were unable to grow on hygromycin B (deletion phenotype), but were only able to grow on nourseothricin (complementation phenotype). Additionally, the presence of the point-mutation in *H3K36A* and *ASH1*$^{H537K}$ mutants was verified by sequencing.

**DNA analysis *via* Southern blot and PCR**

Isolation of plasmid DNA from *S. cerevisiae* FY834 as well as *Escherichia coli* Top10F' (Invitrogen, Darmstadt, Germany) was performed with the NucleoSpin® Plasmid Kit (Macherey-Nagel, Düren, Germany). Furthermore, the isolation of *F. fujikuroi* gDNA from lyophilized and ground mycelium was achieved following the protocol of Cenis (Cenis 1992). Deletion mutants were analyzed for ectopically integrated deletion cassettes *via* Southern blot analysis (Southern 1975). Therefore, gDNA of the mutants and the WT was digested with an appropriate restriction enzyme (Thermo Fisher Scientific, Schwerte, Germany), separated in a 1% (w/v) agarose gel and then transferred to a nylon membrane (Nytran™ SPC, Whatman, Sanford, FL, USA) *via* downward alkali blotting (Ausubel *et al*. 1987). Hybridization of membranes with $^{32}$P-labeled probes, generated with the random oligomer-primer method (Sambrook *et al*. 1989), was performed using 3' flanks (Table S1) as templates. Successful verification of five independent Δ*set2* and six Δ*ash1* mutants can be found in Figures S4B/C and S5B/C, respectively. For amplification by PCR, BioTherm™ DNA Polymerase (GeneCraft, Lüdinghausen, Germany), TaKaRa LA Taq® DNA Polymerase (Takara Bio, Saint-Germain-en-Laye, France) or Phusion® High-Fidelity DNA Polymerase (Finnzymes,

228 Vantaa, Finland) were used. The stability of subtelomeric regions and the accessory
229 chromosome XII was tested with primers listed in Table S3.
230
231 **Clamped homogeneous electric fields (CHEF) gel analysis**
232 Protoplasts of the WT and Δ*ash1* strains were generated as described elsewhere
233 (Tudzynski *et al*. 1999). The protoplasts were resuspended in 1.2% (w/v) InCert agarose
234 (Lonza Group AG, Basel, Switzerland) and run in a 1% (w/v) CHEF gel (Teunissen *et al*.
235 2002). *S. cerevisiae* and *Schizosaccharomyces pombe* chromosomes served as molecular size
236 markers (Bio-Rad, Munich, Germany).
237
238 **Expression analysis *via* quantitative real-time PCR (qRT-PCR)**
239 RNA from lyophilized and ground mycelium was extracted with the TRI Reagent™
240 (Sigma-Aldrich, Steinheim, Germany). For expression analysis by qRT-PCR, 1 µg of
241 DNase I-treated (Thermo Fisher Scientific, Schwerte, Germany) total RNA was transcribed
242 into cDNA using oligo dT primers and SuperScript® II Reverse Transcriptase (Invitrogen,
243 Darmstadt, Germany), and then iQ SYBR Green Supermix (Bio-Rad, München, Germany)
244 was applied for the reaction in a C1000 Touch™ Thermal Cycler with a CFX96™ Real-Time
245 System (Bio-Rad, München, Germany). Transcript levels of regulator genes (*SET2*, *ASH1*,
246 *SET1*, *KDM4*), SM genes (*FSR1*, *BIK1*, *FUS1*, *CPS/KS*), and the constitutively expressed
247 reference genes (*FFUJ_07710*, GDP mannose transporter gene; *FFUJ_05652*, related actin
248 gene; *FFUJ_08398*, ubiquitin gene) were determined in duplicates or triplicates with primers
249 listed in Table S4. With an annealing temperature of 60 °C, primer efficiencies were 90-110%
250 and the results were calculated with the ΔΔCt-method (Pfaffl 2001).
251
252 **Expression analysis *via* microarray**

253 The WT, Δ*set2* T1 and Δ*ash1* T2 were cultivated in ICI medium with 6 mM or 60 mM
254 glutamine for 3 days in duplicates. Total RNA was isolated as described above. However, an
255 additional clean-up step with the NucleoSpin® RNA Clean-up Kit (Macherey-Nagel, Düren,
256 Germany) was performed. The microarrays were designed by Agilent Technologies (Santa
257 Clara, CA, USA), and followed by hybridization performed at Arrows Biomedical (Münster,
258 Germany) according to the manufacturer's protocol. For the heatmaps, the eight different
259 profiles were extracted first, and were then clustered with Perseus 1.5.8.5 (Max Planck
260 Institute of Biochemistry, Martinsried, Germany) (Tyanova *et al*. 2016) using the standard
261 parameters. Genes upregulated in the mutants had a $\log_2$-fold change of ≥ 2 (green),
262 downregulated genes of ≤ -2 (red). The microarray data, additional information on the sample
263 preparation and processing of data are available at the NCBI Gene Expression Omnibus
264 (GEO) under the accession number GSE90947.
265
266 **Western blot analysis**
267 Proteins used for Western blot analysis were extracted from lyophilized and ground
268 mycelium as described elsewhere (Rösler *et al*. 2016). After protein quantification with
269 Bradford Reagent (Sigma-Aldrich, Steinheim, Germany), 15 µg (H3K36me3, H3 C-terminal)
270 or 30 µg (H3K36me2) of the protein extract was separated by sodium dodecyl sulfate
271 polyacrylamide gel electrophoresis using a 15% running gel (Laemmli 1970). Proteins were
272 transferred to a nitrocellulose membrane (Amersham™ Protran™ Premium 0.45 µm NC; GE
273 Healthcare Life Sciences, Little Chalfont, UK) by semi-dry electroblotting, then probing was
274 performed with the following primary antibodies (Active Motif, La Hulpe, Belgium): anti-
275 H3K36me2 (#39256; 1:5,000), anti-H3K36me3 (#61101; 1:10,000) and anti-H3 C-terminal
276 (#39163; 1:10,000). Donkey anti-rabbit IgG-HRP served as secondary antibody (sc-2317;
277 1:10,000; Santa Cruz Biotechnology, Heidelberg, Germany). Chemoluminescence was
278 detected using the NovexVR ECL Chemiluminescent Substrate Reagent Kit (Thermo Fisher

Scientific, Schwerte, Germany). The relative global amount of H3K36me3 in Western blots was determined with a photo editing software (Adobe Photoshop, San Jose, CA, USA): the intensity of the WT band was set to 100% and that of the background to 0%.

**ChIP analysis**

The WT and mutant strains were grown in ICI medium with 6 mM or 60 mM glutamine for 3 days prior to crosslinking with formaldehyde (1%, v/v, final concentration) for 15 min at 28 °C and 90 rpm, and subsequent quenching with glycine (125 mM final concentration) for 5 min at 37 °C. The mycelium was harvested, shock-frozen with liquid nitrogen and ground to powder. Further sample preparation was essentially performed as described elsewhere (Gacek-Matthews *et al*. 2015; Heimel *et al*. 2010). For ChIP-Seq analysis, the cells were lysed using a cell mill (Retsch MM200, 25 Hz, 5 min; Retsch Technology, Haan, Germany) and the chromatin was sonicated using a S220 Focused-ultrasonicator (Covaris, Woburn, MA, USA). Sonication was set to yield DNA fragments with an average size of 150-250 bp. For ChIP-qRT-PCR, the Bioruptor® Plus (Diagenode, Seraing, Belgium) was applied for sonication. The ChIP analyses were done with the anti-H3K36me3 (#61101; Active Motif, La Hulpe, Belgium) and anti-H3K27me3 (#39155; Active Motif, La Hulpe, Belgium) antibodies, then Dynabeads® Protein A (Thermo Fisher Scientific, Schwerte, Germany) was applied for precipitating the chromatin-antibody-conjugate. The WT and Δ*ash1* input samples (strains grown in 60 mM glutamine) were not treated with antibody. One sample each (without replicate) was sequenced with a Genome Sequencer Illumina HiSeq and analyzed bioinformatically at GATC Biotech (Konstanz, Germany). The WT input sample was sequenced at the Karlsruhe Institute of Technology (facility at the Institute of Toxicology and Genetics, Karlsruhe, Germany). For verifying the ChIP-Seq data, ChIP-qRT-PCR of GA, BIK and ubiquitin genes was performed in quadruplicates, using primers that bind at the 3’ gene

ends (Table S4). For H3K27me3, the use of primers binding at the 5' ends of these genes gave very similar results.

Furthermore, we retrieved mapped ChIP-Seq reads from GATC Biotech and calculated normalized locus-specific chromatin state (NLCS) values using EpiChIP (Hebenstreit *et al*. 2011). For each predicted gene, we considered reads that were mapped on the sequence between 1 kb 5'-upstream of the start codon to the stop codon. Genes with a signal probability above 0.95 were defined as significantly enriched for H3K36me3. We applied a quantile normalization on all NLCS values for being able to compare NLCS values between experimental conditions.

**Chemical analysis of SM production**

The WT, Δ*set2*, Δ*ash1* and *H3K36A* mutants were grown in ICI medium with 6 mM (BIK, $GA_3$) or 60 mM (FUS, FSA) glutamine and the WT was grown in ICI with 6 mM $NaNO_3$ (for WT levels of FSR) for 7 days in triplicates. FSR was not produced by Δ*set2* mutants under non-inducing conditions (6 mM glutamine), while BIK produced under this condition by Δ*set2* and WT was extracted from the mycelium (Janevska *et al*. 2016) and taken up in 20 µL dimethyl sulfoxide + 0.75 mL acetonitrile (20%, v/v). BIK and FSR produced by Δ*ash1* and *H3K36A* mutants (6 mM glutamine) were directly analyzed in comparison to the WT (6 mM glutamine, 6 mM $NaNO_3$). FUS and FSA were also directly measured without further processing; the supernatant was filter-sterilized using 0.45 µm membrane filters (BGB Analytik, Schloßböckelheim, Germany). $GA_3$ was extracted and concentrated from 20 mL supernatant with Sep-Pak $C_{18}$ cartridges (Waters, Eschborn, Germany) and subsequent elution with 2 mL acetonitrile (55%, v/v). Analysis *via* high performance liquid chromatography coupled to diode array detection (HPLC-DAD) of BIK, FSR, FUS and FSA was essentially performed as described by Studt *et al*. 2012, while HPLC-DAD analysis of $GA_3$ was carried out as described by Wiemann *et al*. 2012, both analyses on a VWR Hitachi Chromaster HPLC

system (VWR International, Darmstadt Germany) with a EZChrome Elite 3.3.2 SP2 software (Agilent Technologies, Santa Clara, CA, USA). The production of all metabolites was related to the dry weight of the strains. For this purpose, the mycelium was harvested, freeze-dried and weighed.

### Rice pathogenicity assay

The infection of surface-sterilized seedlings of *Oryza sativa* spp. *japonica* cv. Nipponbare with mycelial plugs of WT, Δ*set2* T1 and Δ*ash1* T2 was performed as described elsewhere (Janevska *et al*. 2017). The gDNA of four infected and lyophilized rice roots per sample was extracted using the NucleoSpin® Plant II Kit (Macherey-Nagel, Düren, Germany) according to the manufacturer's instructions. The fungal gDNA was normalized against the plant gDNA, both quantified by qRT-PCR using the ΔCt method (Livak and Schmittgen 2001) as well as primer pairs BIK1_3'ChIP_F/BIK1_3'ChIP_R and ITS1P/ITS4 (Table S4), respectively (Studt *et al*. 2017). The annealing temperatures were 62 °C and 55 °C for *BIK1* and *ITS*, respectively.

### Data availability

Sequence data are available at GenBank and the relevant accession numbers can be found throughout the text and in Tables S1-S4. Microarray expression data are available at GEO with the accession number GSE90947.

## Results

### Identification of the *F. fujikuroi* H3K36 methyltransferases Set2 and Ash1

A BLASTp search with the extracted SET domain (InterPro IPR001214) of *S. cerevisiae* S288C Set2 (NCBI NP_012367) (Strahl *et al*. 2002) revealed two homologs in *F. fujikuroi* (Figure 1A). The amino acid sequence of the SET domain of *S. cerevisiae* Set2 is 63% and 42% identical to the SET domains of FFUJ_08690 and FFUJ_05655, respectively. The visualization of the protein domains of these two putative histone methyltransferases showed that they share the typical SET domain organization of members of the H3K36-specific Set2 family, namely a combination of SET, Associated with SET and Post-SET domains (Figure 1A/B) (Adhvaryu *et al*. 2005; Brosch *et al*. 2008). Furthermore, FFUJ_08690 was identified as the direct yeast Set2 homolog due to the presence of additional conserved domains, *i.e.* the RNA polymerase II interaction domain (Set2 Rbp1 interacting, SRI) and the WW/Rsp5/WWP domain with two conserved tryptophan residues, possibly involved in protein-protein interaction (Brosch *et al*. 2008; Gao *et al*. 2006; Kizer *et al*. 2005; Strahl *et al*. 2002). Therefore, FFUJ_08690 was designated as *F. fujikuroi* Set2 (Figure 1A).

A BLASTp search with the second Set2 homolog FFUJ_05655 showed that it has high similarity to a second member of the Set2 family, the H3K36-specific methyltransferase Ash1 (*Drosophila* discs absent, small, or homeotic-1) identified in higher eukaryotes, including *D. melanogaster* (Tanaka *et al*. 2007). The SET domain of *D. melanogaster* Ash1 (GenBank AAB01100) is 47% and 37% identical to the SET domains of FFUJ_05655 and *F. fujikuroi* Set2 (FFUJ_08690), respectively. Therefore, FFUJ_05655 was designated as *F. fujikuroi* Ash1 (Figure 1A). It is noteworthy that *F. fujikuroi* Ash1 is much shorter when compared to the *D. melanogaster* Ash1 homolog (786 *vs.* 2210 amino acids) which harbors additional domains, *i.e.* a plant homeodomain (PHD)-type zinc finger (IPR001965) and a Bromo adjacent homology domain (IPR001025) (Tanaka *et al*. 2007). A bioinformatic analysis performed by Brosch *et al*. confirmed that filamentous fungi, such as *A. nidulans*, *N. crassa* and *Ustilago maydis*, but not the fission yeast *S. pombe*, encode two homologs of the Set2

family (Brosch *et al*. 2008). However, the Ash1 homolog has not been analyzed for filamentous fungi so far.

Single and double deletion mutants were successfully generated for *SET2* and *ASH1*. Furthermore, the target lysine residue of these putative H3K36 methyltransferases was exchanged for alanine, gaining *H3K36A* mutants, which can neither be methylated nor acetylated at this residue. First of all, the global H3K36 methylation level in these mutants was compared to that of the WT *via* Western blot analysis using the specific antibodies for H3K36me3 and H3K36me2. While the global H3K36me3 level was strongly reduced (17-28% left) in Δ*set2* transformants (T), it was only slightly affected (60-76% left) upon deletion of *ASH1* (Figure 1C). The global H3K36me2 level was marginally reduced in both deletion backgrounds, suggesting that Set2 and Ash1 almost equally contribute to global H3K36me2 levels (Figure 1C). The H3K36me3 signal was fully abolished in the Δ*set2*/Δ*ash1* double deletion and the *H3K36A* mutants as expected (Figure 1C/D). Judging from the obtained signal intensities, it can be assumed that the H3K36me3 mark is more abundant than the H3K36me2 mark in *F. fujikuroi* (Figure 1C). Similarly, a mass spectrometric analysis of histone proteins in *A. nidulans* showed that 28% and 64% of H3 proteins carried K36me2 and K36me3 modifications, respectively (Gacek-Matthews *et al*. 2015). H3K36 acetylation was hardly detected in the *F. fujikuroi* WT, as shown earlier (Rösler *et al*. 2016), and was therefore not analyzed in the mutants by Western blot analysis.

Summarizing, Set2 and Ash1 are the only H3K36-specific methyltransferases in *F. fujikuroi*, and Set2 contributes with a considerably higher extent to the global H3K36me3 level compared to Ash1.

**Deletion of *SET2* and *ASH1* strongly affects vegetative growth and conidiation**

Next, we analyzed the impact of *SET2* and *ASH1* single and double deletions as well as *H3K36A* mutation on the vegetative growth of *F. fujikuroi*. A plate assay with complex and

minimal media showed a growth defect for all strains on all tested media, in which the Δ*ash1* mutants exhibited the most severe phenotype with the strongest reduction in colony diameter (Figure 2A). This was especially interesting, as the global level of H3K36me3 was only slightly reduced upon deletion of *ASH1* (Figure 1C/D). Surprisingly, the growth defect of the double deletion and the *H3K36A* mutants was less severe compared to the Δ*ash1* single deletion mutant (Figure 2A/B). *In loco* complementation of the mutants with the respective native genes restored normal vegetative growth (Figure S7A/C/D). Besides, both Ash1 and Set2 were shown to be required for conidiation, because formation of microconidia was almost fully abolished in all mutants (Figure S7E).

In order to elucidate whether the methyltransferase activity of Ash1 is required to fully complement the Δ*ash1* phenotype, we introduced a gene copy carrying a point mutation within the SET domain of Ash1 (H537K), gaining $ASH1^{H537K}$ mutants, as described for the *Drosophila ASH1* gene (Tanaka *et al*. 2007). Complementation of Δ*ash1* with $ASH1^{H537K}$ neither restored the H3K36 methylation defect (Figure S7B), nor the growth defect (Figure S7A). Therefore, the observed growth defect of Δ*ash1* is most likely due to the loss of function as methyltransferase.

In summary, all analyzed mutants showed more (Δ*ash1*) or less (Δ*set2*, Δ*set2*/Δ*ash1*, *H3K36A*) severe growth defects. Both Ash1 and Set2 are essential for conidia formation.

**Ash1 deposits H3K36me3 at subtelomeric regions contributing to their stability**

In order to gain deeper insight into the distribution of H3K36me3 in *F. fujikuroi* and to further analyze the role of Ash1 in its deposition, we performed ChIP-Seq using an H3K36me3 antibody. We cultivated the WT and one of the Δ*ash1* mutants (T2) in the presence of limiting (6 mM, N-) and saturating (60 mM, N+) amounts of glutamine, conditions that are important for the biosynthesis of different SMs. As a control, the WT and Δ*ash1* input samples, which had not been treated with antibody, were sequenced and therefore

represent a whole-genome sequencing of these strains. The ChIP-Seq experiment revealed that H3K36me3 is covering entire chromosomes in *F. fujikuroi*, shown for chromosomes I, X and XII (Figure 3) and chromosomes II, V and XI (Figure S8).

Comparing the distribution of H3K36me3 marks along the chromosomes between the WT and the Δ*ash1* mutant showed a significant reduction of this mark at subtelomeric regions in the mutant. In addition, sequencing of the Δ*ash1* input sample revealed the absence of two subtelomeric regions of chromosomes I and X in this mutant (Figure 3A/B) suggesting that H3K36me3 deposited by Ash1 directly or indirectly influences chromosome stability. PCR analysis of five additional Δ*ash1* transformants showed that a loss of the outermost gene (*FFUJ_11196*) close to the telomere of chromosome X occurred in five out of six independent primary transformants, while a larger region of ca. 430 kb up to *PKS14* (*FFUJ_11034*) was missing in three out of six transformants (Figure 3B). The smallest chromosome, the accessory chromosome XII, was shown to be strongly depleted in H3K36me3 in Δ*ash1* T2, which seems to influence its stability. This was underlined by the complete loss of chromosome XII in Δ*ash1* T30, which was shown by PCR using primers for genes close to the telomeres (*FFUJ_14091*; *FFUJ_14261*) and close to the centromere (*FFUJ_14235*; *FFUJ_14241*) of chromosome XII (Figure 3C). Detailed sequence analysis of the ChIP-Seq data of the Δ*ash1* input sample revealed the presence of novel telomeric repeats at the breakage points of chromosomes I and X: five conserved repeats of "TAGGGT" were identified, but the novel telomeres are likely to extend beyond that region (Figure 3A/B).

Intrigued by these findings, we performed an experimental evolution approach by directly observing the process of gene losses at work. We analyzed the presence of subtelomeric genes of all twelve chromosomes after 20 generations with 3 days of growth per generation, *i.e.* after 60 days of growth on solid complex medium. Further losses were observed for one, or several, of the six independent Δ*ash1* mutants on chromosomes V, VI, VIII and IX. Furthermore, the accessory chromosome XII was now missing in three out of six mutants

(Figure S9A). Only small phenotypic differences concerning the vegetative growth of the strains were observed after the 20 passages (Figure S9E). In contrast, no losses of subtelomeric genes were found for five independent Δ*set2* mutants (Figure S9B) and six independent Δ*set2*/Δ*ash1* double mutants (Figure S9D). Chromosome XII was missing only in one out of five independent *H3K36A* mutants (Figure S9C), suggesting that the observed genomic instability is characteristic only for *ASH1* single mutants. In order to further elucidate Δ*ash1* chromosome structure, pulse field gel electrophoresis (PFGE) combined with clamped homogeneous electric fields (CHEF) was performed for three initial and six evolved strains of Δ*ash1* in comparison to the WT. No major differences were found for the nine strains, excluding gross chromosomal rearrangements (Figure S10). However, the CHEF gel verified the loss of the smallest chromosome XII in some of the strains, and the loss of the outer part of chromosome X (432 kb in the sequenced strain Δ*ash1* T2) resulting in a shift of its size (Figure S10).

Taken together, single deletion of *ASH1*, but not of *SET2* or the respective double deletion, resulted in losses of subtelomeric regions and/or loss of the dispensable chromosome XII. The ongoing losses of subtelomeric regions after 20 passages of Δ*ash1* mutant strains to fresh medium suggest that Ash1 contributes to genomic stability.

**Transcriptome analysis of *SET2* and *ASH1* deletion mutants**

In yeast, it has been shown that Set2 interacts with the elongating form of RNA polymerase II, thereby affecting gene expression (Krogan *et al*. 2003). To investigate how H3K36 methylation by Set2 and Ash1 affects mRNA transcription in *F. fujikuroi*, we performed a genome-wide microarray expression analysis, cultivating the WT, Δ*set2* T1 and Δ*ash1* T2 mutants in the presence of 6 mM and 60 mM glutamine. Based on the selection criteria of a 4-fold change in expression ($log_2$-fold change ≥ 2 or ≤ -2) at the 95% confidence interval (False Discovery Rate < 0.05), 4,087 of the 14,816 annotated genes (27.6%) were

affected in a Set2- and/or Ash1-dependent manner in at least one condition. 3,134 and 2,170 genes were affected under nitrogen-limitation and nitrogen-surplus conditions, respectively (Figure 4A/B), so that an overlap of 964 genes were regulated under both conditions. A larger number of genes were shown to be regulated (directly or indirectly) by Set2 and Ash1 in a similar manner. For example, in the presence of 6 mM glutamine, 550 and 374 genes were up- and downregulated in both Δs*et2* and Δ*ash1*, respectively, while only 28 genes were regulated by Set2 and Ash1 in an antagonistic manner (Figure 4A).

Interestingly, a great number of genes encoding putative TFs and histone modifying enzymes were identified as direct or indirect target of Set2 and Ash1. 281 TF- and 34 histone modifier-encoding genes were 4-fold up- or downregulated in at least one strain under at least one condition (Figure S11A). Furthermore, *SET2* and *ASH1* were found to be downregulated in both Δ*ash1* and Δ*set2*, respectively (Figure S11B/C), indicating a negative feedback on the transcription of *SET2* when *ASH1* is missing, and *vice versa*. Furthermore, the putative H3K4 methyltransferase gene *SET1*/*FFUJ_02475* (Liu *et al*. 2015) was downregulated in Δ*ash1* (Figure S11B/C), indicating a cross-talk between histone modifiers on a transcriptional level. Additionally, these data suggest that many of the observed phenotypic effects of *SET2* and *ASH1* deletion may be indirect indeed, *i.e.* they might be mediated by unknown downstream targets of Set2 and Ash1.

To evaluate whether the deposition of H3K36me3 correlates with active transcription in *F. fujikuroi*, we calculated the degree of chromatin modification per gene in terms of normalized locus-specific chromatin state (NLCS) values (Hebenstreit *et al*. 2011). After that, we correlated the fold changes in NLCS values to gene expression fold changes between Δ*ash1* and WT in the presence of 6 mM and 60 mM glutamine. For both comparisons, we could not determine a significant correlation between H3K36me3 modification and gene expression (Pearson = -0.0228 for 6 mM glutamine; Pearson = -0.0065 for 60 mM glutamine) (Figure S12). We also compared the distribution of gene expression of genes with a

significant chromatin modification signal (signal probability > 95%) to genes without significant signal. For 6 mM and 60 mM glutamine, no significant difference between the two distributions could be determined (Figure S13).

Taken together, both histone methyltransferases directly or indirectly influence the expression of 4,087 out of the 14,816 annotated genes in *F. fujikuroi*, including a large set of TF- and histone modifier-encoding genes. However, the H3K36 methylation pattern does not correlate with transcriptional activity.

**Deregulation of secondary metabolism upon deletion of *SET2* and *ASH1***

Among the genes affected by single deletion of *SET2* and/or *ASH1* were several known and yet uncharacterized putative SM key genes (Figure S14A/B). As already reflected in the overall transcriptome (Figure 4), most of the SM key genes were up- or downregulated in both Δ*set2* and Δ*ash1*, and therefore were regulated (directly or indirectly) in a similar manner by the two methyltransferases (Figure S14A). Among the cryptic SM key genes without an assigned product, *PKS-NRPS9* (*FFUJ_14695*) and *NRPS4* (*FFUJ_08113*) were shown to be upregulated in both Δ*set2* and Δ*ash1* (Figure S14A).

To further evaluate the impact on secondary metabolism, Δ*set2*, Δ*ash1* and *H3K36A* mutants were grown in comparison to the WT under SM-inducing conditions and the SM levels were determined *via* HPLC-DAD. First of all, the biosynthesis of the two red pigments BIK and FSR was analyzed. While BIK production was unaffected upon deletion of *SET2*, it was downregulated in Δ*ash1* and *H3K36A* mutants under its favorable culture condition (6 mM glutamine, acidic pH) (Wiemann *et al*. 2009). At the same time, FSR production was deregulated in Δ*ash1* and *H3K36A*, accumulating under non-favorable acidic conditions (Figure 5A). In the WT, FSR gene expression and product formation are induced in the

presence of limiting amounts of nitrate (6 mM $NaNO_3$), conferring an alkaline ambient pH (Studt *et al*. 2012).

Concerning the biosynthesis of the mycotoxins FUS and FSA, their production was upregulated 2- to 5-fold in all mutants under their favorable culture condition, 60 mM glutamine (Niehaus *et al*. 2013; Niehaus *et al*. 2014) (Figure 5B). The production of the bioactive phytohormone $GA_3$ was shown to be downregulated in all mutants: $GA_3$ production was not detected in Δ*ash1* mutants and $GA_3$ levels were down to ca. 5% in Δ*set2* in comparison to the WT (Figure 5C). SM production levels correlated well with the microarray expression analysis of SM genes for Δ*set2* and Δ*ash1* (Figure S14A/B).

Next, H3K36me3 levels were analyzed for the WT and the Δ*set2*, Δ*ash1* and *H3K36A* mutants at the GA and BIK gene clusters (subtelomeric regions) and at the euchromatic ubiquitin gene for direct comparison by ChIP with subsequent qRT-PCR. Furthermore, a possible cross-talk to the heterochromatic mark H3K27me3 was evaluated, which has been described for human cells (Yuan *et al*. 2011). The analysis verified the ChIP-Seq data and showed that H3K36me3 at the GA cluster is deposited by Ash1, while H3K36me3 at the BIK cluster is Set2-derived (Figure 6A/B; Figure 7A). Intriguingly, an increase in the heterochromatic mark H3K27me3 was observed for both the GA and BIK cluster in the Δ*ash1*, but not in the Δ*set2* or *H3K36A* mutants (Figure 7B). In fact, GA and BIK clusters can be found at subtelomeric regions of facultative heterochromatin at chromosome V (*DTC1*, *PKS4*; Figure S8B), regions that are generally targeted by Ash1 as described above. In contrast, H3K27me3 was not increased at the euchromatic ubiquitin gene in Δ*ash1*, which lies in a region that is H3K36-methylated by Set2 (Figure 6C; Figure 7A/B).

No correlation between the deposition of these two methylation marks (ChIP-qRT-PCR) and GA or BIK product formation (HPLC-DAD) was found: all mutants showed a reduced GA production, but only Δ*ash1* and *H3K36A* had lower levels of H3K36me3, while Δ*ash1* additionally accumulated increased levels of H3K27me3 at GA cluster genes (Figure 5C;

Figure 7A/B). Moreover, both Δ*ash1* and *H3K36A* showed a reduced BIK production, but *H3K36A* had lower levels of H3K36me3, whereas Δ*ash1* had higher levels of H3K27me3 at BIK cluster genes (Figure 5A; Figure 7A/B).

Furthermore, little correlation between the deposition of H3K36me3 (ChIP-Seq) and the transcription of GA and BIK cluster genes (microarray) was observed for the WT and Δ*ash1*: in the WT, the mark was found under both limiting and saturating amounts of glutamine, while GA and BIK genes were only expressed under nitrogen limitation (Figure 6A/B). Moreover, in Δ*ash1*, an upregulation of BIK genes was detected under non-favorable high nitrogen conditions, possibly correlating with enhanced levels of H3K36me3 (Figure 6B). However, this did not result in an efficient production of the red pigment under non-favorable conditions, judging from HPLC-DAD analyses and the pigmentation of the flasks (Figure S15A/B).

In summary, a large impact on secondary metabolism was detected upon deletion of *SET2* and *ASH1*, although the effects are likely to be indirect and not mediated *via* H3K36me3 or H3K27me3 levels at the gene clusters (tested for GA and BIK). Only in Δ*ash1*, but not in Δ*set2* or *H3K36A* mutants, elevated levels of H3K27me3 were detected at subtelomeric regions.

**Deletion of *SET2* and *ASH1* results in an attenuated pathogenicity on rice**

*F. fujikuroi* causes *bakanae* disease of rice due to its ability to produce GAs, a family of plant hormones. As Δ*ash1* and Δ*set2* mutants showed a fully or almost fully abolished production of $GA_3$, respectively (Figure 5C), we performed a pathogenicity assay on rice. Healthy rice seedlings were infected with mycelium of the WT, Δ*set2* T1 and Δ*ash1* T2. Infection with the deletion mutants did not result in the chlorotic, thin, curled and hyper-elongated internodes of rice, while infection with the WT showed this characteristic *bakanae* symptom (Figure 8A). Nevertheless, rice plants infected with Δ*ash1*, and especially Δ*set2*,

589 differed from the non-infected plants ($H_2O$ negative control) by their extended internodes
590 (Figure 8A). These data suggest that minimal amounts of GA are produced *in planta* by
591 Δ*ash1* and Δ*set2* in contrast to *in vitro* conditions (Figure 5C). The quantification of the
592 fungal DNA within infected rice roots by qRT-PCR revealed that Δ*set2* and especially Δ*ash1*
593 mutants were not as efficient in colonizing the rice roots as the WT (Figure 8B).
594
595 **_F. fujikuroi_ Kdm4 is an H3K36-specific demethylase**
596 To analyze the putative antagonist for H3K36me3 deposited by *F. fujikuroi* Set2 and
597 Ash1, we performed a BLASTp search to identify the *F. fujikuroi* homolog of the JmjC
598 demethylase KdmA that has been described for *A. nidulans* FGSC A4 (Gacek-Matthews *et al*.
599 2015). The overall amino acid identity between *A. nidulans* KdmA (AN1060) and
600 FFUJ_01769, the only identified homolog, is 47% with a query cover of 63%. However, the
601 homology of the extracted JmjC catalytic domains (IPR003347) is much higher, having an
602 amino acid identity of 79%. Furthermore, *A. nidulans* KdmA and *F. fujikuroi* FFUJ_01769
603 show a conserved domain structure, both additionally harboring JmjN (IPR003349) and PHD-
604 type zinc finger (IPR001965) domains (Gacek-Matthews *et al*. 2015). Therefore, FFUJ_01769
605 was designated as *F. fujikuroi* Kdm4 according to the general nomenclature (Allis *et al*.
606 2007).
607 Single deletion mutants of *KDM4* were generated and analyzed for their vegetative
608 growth, conidiation and SM production in comparison to the WT. A plate assay with complex
609 and minimal media showed a WT-like growth for independent Δ*kdm4* mutants (Figure S16A).
610 The plate assay was repeated under increasing light conditions and in the presence of
611 0-40 mM $H_2O_2$ to induce oxidative stress. However, no phenotypic difference was observed
612 compared to the WT also under these stress conditions (Figure S16B). Furthermore, SM
613 production of BIK, FUS, FSA and $GA_3$ was unaffected upon deletion of Δ*kdm4* (Figure
614 S17B). Only a slight effect on sporulation was observed, with Δ*kdm4* mutants consistently

producing 3- to 4-times more conidia than the WT in independent experiments (Figure S17A). Indeed, there was no upregulation of the global H3K36me3 level upon deletion of *KDM4* within the detection limits of the performed Western blot analysis (Figure S17C), which likely explains the mild phenotype observed.

In contrast, constitutive overexpression of *KDM4 via* the strong *PoliC* promoter from *A. nidulans* exhibited the most severe phenotype, as several rounds of purification *via* protoplast generation and selection on the resistance marker hygromycin B were insufficient to gain stable overexpression strains. OE::*KDM4* mutants showed a severe growth defect on complex medium in the presence of hygromycin B, however, this phenotype was completely lost when grown in its absence (Figure S3A). Real-time expression analysis revealed that *KDM4* was not overexpressed when the strains were grown in the absence of hygromycin B (Figure S3B), and PCR analysis verified that the construct was lost in the absence of the resistance marker (Figure S3C/D). A Western blot analysis with two independent OE::*KDM4* transformants grown in the presence of hygromycin B showed a decreased level of global H3K36me3 (Figure S3E), providing evidence that Kdm4 represents the H3K36-specific demethylase also in *F. fujikuroi*. Unfortunately, due to the instability of the overexpression construct, further phenotypic analyses with OE::*KDM4* mutants were not feasible. Taken together, *F. fujikuroi* Kdm4 is the H3K36me3-specific antagonist to Set2 and Ash1.

## Discussion

### Set2 and Ash1 are two H3K36-specific histone methyltransferases

In the present work, we describe the characterization of two H3K36-specific histone methyltransferases in *F. fujikuroi*, designated Set2 and Ash1. Judging from the Western blot and ChIP-Seq analyses, Set2 represents the major H3K36 methyltransferase, depositing the majority of H3K36me3, whereas Ash1 contributes to the global H3K36me3 level to a lesser

extent. Both Set2 and Ash1 contribute to the global H3K36me2 level, however, this mark is less abundant in *F. fujikuroi*, a feature which has also been shown for *A. nidulans* (Gacek-Matthews *et al*. 2015). The double deletion of *SET2* and *ASH1* resulted in total loss of H3K36me3, demonstrating that no additional H3K36 methyltransferase is present in *F. fujikuroi*.

While there is only one H3K36-specific methyltransferase in budding and fission yeasts, there are two members of the Set2-family in filamentous fungi (Brosch *et al*. 2008). However, only the Set2 homolog has been studied so far: in *N. crassa* and *F. verticillioides*. While there was residual H3K36me3 methylation upon deletion of *F. verticillioides SET2* (Gu *et al*. 2017), *N. crassa* Set2 seems to account for all of the detected H3K36me2/me3 methylation (Adhvaryu *et al*. 2005). In the latter case, the Ash1-mediated H3K36 methylation in the *N. crassa SET2* deletion background may not have been detected due to the limitations of the performed Western blot analysis (Adhvaryu *et al*. 2005). Interestingly, the *F. fujikuroi* Δ*set2*/Δ*ash1* double deletion and the *H3K36A* mutants were viable despite the complete loss of all detectable H3K36me2/me3, whereas a comparable H3 mutation of lysine to leucine (*H3K36L*) in *N. crassa* was not (Adhvaryu *et al*. 2005).

Although Set2 and Ash1 were shown to be specific H3K36 methyltransferases, it cannot be excluded that they have further targets and can also methylate non-histone proteins, as shown for the human H3K36 methyltransferase NSD1 (Lu *et al*. 2010).

**Set2 and Ash1 deposit H3K36me3 at specific loci which is ubiquitous in *F. fujikuroi***

The ChIP-Seq analysis revealed that every single *F. fujikuroi* chromosome harbors the H3K36me3 mark and that it is enriched in nearly every single gene. Very similar results were obtained for *A. nidulans* and *F. graminearum via* mass spectrometry and ChIP-Seq analyses, respectively (Connolly *et al*. 2013; Gacek-Matthews *et al*. 2015).

The ChIP-Seq analysis of the *F. fujikuroi* Δ*ash1* mutant strongly indicates that Set2 and Ash1 each deposit their H3K36me3 at very specific loci. The Ash1-mediated H3K36 methylation (lost in Δ*ash1*) was mainly found in subtelomeric regions of facultative heterochromatin, while the remaining Set2-mediated H3K36 methylation was present within euchromatic regions. Comparing the present ChIP-Seq data with those of H3K4me2 (and ChIP-qRT-PCR of H3K4me3), H3K9me3 and H3K27me3, which were generated for *F. fujikuroi* under comparable culture conditions (Studt *et al*. 2016a; Studt *et al*. 2017; Wiemann *et al*. 2013), we can draw the following conclusions: 1) Very little H3K9me3 methylation is present and can be mainly found at centromeric regions, making up the constitutive heterochromatin of *F. fujikuroi* centromeres (Wiemann *et al*. 2013). Therefore, this silencing mark rarely overlaps with any other of the analyzed histone marks. 2) Within euchromatic regions, an enrichment of the activating marks H3K4me2/me3 was identified, and these regions exactly overlap with H3K36me3 deposited by Set2 (Studt *et al*. 2017; Wiemann *et al*. 2013). In *S. cerevisiae*, all euchromatic genes carried H3K4me2, while H3K4me3 was a sign of actively or recently performed gene expression (Ng *et al*. 2003; Santos-Rosa *et al*. 2002). 3) Within subtelomeric regions of facultative heterochromatin, an enrichment of the silencing mark H3K27me3 was found (Studt *et al*. 2016a), which rarely overlaps with H3K4me2/me3, but exactly overlaps with H3K36me3 deposited by Ash1 (Figure 9).

Thus, Set2-mediated H3K36me3 co-exists with H3K4me2/me3, and Ash1-mediated H3K36me3 co-exists with H3K27me3 (Figure 9). In contrast, H3K4me2/me3 and H3K27me3 rarely overlap. The same is true for *F. graminearum* where only 627 genes (of all annotated 13,354 genes) were considered as bivalent regions carrying both H3K4 and H3K27 methylation marks (Connolly *et al*. 2013). Therefore, H3K4me2/me3 and H3K27me3 characterize stretches of euchromatin and facultative heterochromatin, respectively, while H3K36me3 is virtually ubiquitous. Comparing the ChIP-Seq and expression data, no

692 significant correlation between H3K36me3 and active transcription was found in *F. fujikuroi*
693 (this work) and *F. graminearum* (Connolly *et al*. 2013).

694 This interesting result stands in marked contrast to the bulk of published data for budding
695 and fission yeasts and higher eukaryotes, *e.g. Arabidopsis thaliana* (Xu *et al*. 2008),
696 *D. melanogaster* (Bell *et al*. 2007; Wang *et al*. 2013), chicken (Bannister *et al*. 2005) and
697 human cells (Barski *et al*. 2007; Miao and Natarajan 2005; Schwämmle *et al*. 2014; Vakoc *et*
698 *al*. 2006; Yuan *et al*. 2011). In these organisms, it has been established that both H3K4 and
699 H3K36 methylation marks are specific and characteristic hallmarks of actively transcribed
700 euchromatin, whereas H3K9 and H3K27 methylation characterizes silenced stretches of
701 heterochromatin (Rando and Chang 2009).

702 Therefore, the amount and location of H3K36 methylation seems to be different in
703 *F. fujikuroi*, and likely also in other filamentous fungi, and we suggest that H3K36me3
704 deposited by Set2 and Ash1 exerts specific and distinct functions as described below.

705

706 **Set2 likely interacts with RNA polymerase II while Ash1 may be involved in the repair**
707 **of double strand breaks**

708 One well-established function for Set2 homologs, including the ones characterized in
709 *S. cerevisiae* and humans, is the interaction with the elongating form of RNA polymerase II
710 *via* its SRI domain (Kizer *et al*. 2005; Krogan *et al*. 2003; Li *et al*. 2005; Sun *et al*. 2005).
711 This is likely to be true also for *F. fujikuroi* Set2 as it contains the conserved SRI domain
712 (Figure 1A; Figure 9), while *F. fujikuroi* Ash1 does not. Furthermore, the H3K36me3 pattern
713 deposited by *F. fujikuroi* Set2 within euchromatic regions shows characteristic peaks towards
714 the 3’ end of each gene, but not in intergenic regions, as depicted for the ubiquitin-encoding
715 reference gene (Figure 6C). This accumulation of H3K36me3 within gene bodies of actively
716 transcribed genes is characteristic for Set2-mediated deposition *via* interaction with RNA
717 polymerase II (Krogan *et al*. 2003; Pokholok *et al*. 2005; Vakoc *et al*. 2006).

In contrast, H3K36me3 derived from Ash1 at subtelomeric regions shows no outstanding peak towards 3' ends of genes but is more diffused and often also found in intergenic regions, as highlighted for the GA gene cluster (Figure 6A). Consistently, a characteristic phenotype for Δ*ash1* mutants has been identified, namely the progressive loss of subtelomeric regions and of the whole accessory chromosome XII depleted in Ash1-mediated H3K36me3. The chromosome instability was already shown for primary transformants of Δ*ash1*, and additional losses of subtelomeric regions were observed after several passages of growth on solid medium. Our data are consistent with observations made for higher organisms: H3K36 methylation is involved in DNA repair and the maintenance of genomic stability, including mismatch repair as well as the repair of double strand breaks in the mammalian system (Duns *et al*. 2010; Fnu *et al*. 2011; Li *et al*. 2013; Pfister *et al*. 2014). We suggest that H3K36me3 formation by *F. fujikuroi* Ash1 may be involved in similar DNA repair processes (Figure 9). In this regard, the complete loss of the accessory chromosome XII may be attributed to the fact that it is very small and nearly completely heterochromatic (Studt *et al*. 2016a; Wiemann *et al*. 2013) and therefore, nearly completely targeted by Ash1.

Similar losses as in Δ*ash1* mutants were not characteristic for *H3K36A* mutants (only chromosome XII was missing in one out of five *K3K36A* mutants) or Δ*set2*/Δ*ash1* double mutants, which were both completely depleted in H3K36me3. Only for Δ*ash1*, but no other strain, an increased level of H3K27me3 at subtelomeric regions was detected, a cross-talk which seems to require the presence of Set2-mediated, euchromatic H3K36me3. In human cells, Ash1-mediated H3K36 methylation has been shown to counteract H3K27 methylation. The reason for this interference is that H3K36 methylation directly inhibits the H3K27-methylating Polycomb repressive complex 2 *in vitro* and *in vivo* (Yuan *et al*. 2011). It is tempting to hypothesize that something similar might be true for *F. fujikuroi* Ash1. In this case, Ash1 might be involved in keeping the H3K27me3 level as low as possible. In general, regions enriched for H3K27me3, such as subtelomeric regions or accessory chromosomes, are

regions of great diversity, recombination and rearrangements, frequently accumulating single nucleotide polymorphisms (Connolly *et al*. 2013; Schotanus *et al*. 2015). One can speculate that H3K36me3 at these regions might be required to counteract these processes.

Intriguingly, the analysis of the ChIP-Seq data of Δ*ash1* T2 indicated how the broken chromosomes can be "healed", as new telomeric repeats were identified at the breakage points of chromosomes I and X, most likely *de novo* synthesized by a telomerase (Lundblad 2001). An additional way to heal a broken chromosome would be through break-induced replication, in which the broken chromosome invades an intact chromosome *via* a region of low homology, so that it receives the duplicated chromosome end including a telomere (Lundblad 2001). No duplicated regions were identified in the Δ*ash1* T2 ChIP-Seq data, and no dramatic changes of chromosome sizes have been observed, so that this pathway can be excluded.

**Deletion of *SET2* and *ASH1* affects growth, conidiation and SM production**

Phenotypic analyses of Δ*set2* and Δ*ash1* mutants showed a significantly impaired growth on solid media as well as an inability to produce conidia. Deletion of *N. crassa SET2* also resulted in slow growth and poor conidiation (Adhvaryu *et al*. 2005). Accordingly, *F. fujikuroi* Δ*kdm4* exhibited an enhanced conidia production in comparison to the WT, probably due to an enhanced level of H3K36me3 at specific loci, although there was no increase in the global methylation level. Therefore, it is tempting to hypothesize that the decrease of H3K36me3 in Δ*set2* and Δ*ash1* mutants exerts a direct or indirect effect on conidiation-related genes.

Intriguingly, Δ*set2* and Δ*ash1* mutants showed a similar phenotype with regard to their SM profiles: both mutants produced more FUS and FSA, but less GAs compared to the WT. The SM gene clusters are mainly located in regions of facultative heterochromatin, which seems to be primarily associated with Ash1-deposited H3K36me3. As shown above, Set2 and

Ash1 mainly perform their methylation at distinct parts of the chromosomes. Therefore, it is difficult to understand why both deletion mutants show such a similar phenotype concerning their SM biosynthesis. In the present work, no correlation between the deposition of H3K36me3 or H3K27me3 (*via* ChIP-qRT-PCR) and the production of GA and BIK (*via* HPLC-DAD) in Δ*set2*, Δ*ash1* and *H3K36A* mutants could be detected. Therefore, many of the effects are likely to be secondary, due to the large number of direct or indirect downstream TFs and histone modifiers that were identified in the microarray expression analysis.

In addition, both mutants showed a significantly impaired virulence on rice, most likely as a result of their downregulated GA biosynthesis. However, a residual GA production can be assumed for Δ*ash1 in planta*, because this mutant was still able to penetrate the rice roots and induce an elongation of the rice internodes, though without inducing the typical yellowish and pale green leaves (Wiemann *et al*. 2013). Therefore, yet unknown *in planta* signals allow GA production in rice in contrast to the *in vitro* conditions. Similar results were shown for the regulatory mutant Δ*sge1*, encoding a major regulator of secondary metabolism in *F. fujikuroi* (Michielse *et al*. 2015).

**Kdm4 antagonizes H3K36me3 and possibly H3K9me3**

Besides the two H3K36 methyltransferases, we analyzed their counterpart, the *F. fujikuroi* JmjC demethylase Kdm4. The constitutive overexpression of *KDM4* showed the most severe phenotype, because no stable overexpression strains could be gained. Keeping in mind that the Δ*set2*/Δ*ash1* and *H3K36A* mutants were viable despite the complete lack of all H3K36 methylation, the severe phenotype of the OE::*KDM4* mutants can only be explained by an additional role of Kdm4 in the regulation of gene expression, possibly through the interaction with other regulators. Alternatively, this phenotype could be caused by the demethylation of H3K9me3 by Kdm4, as H3K9 demethylation has been shown to be conserved for the human and yeast enzymes (Klose *et al*. 2006; Klose *et al*. 2007). So far, no

viable deletion mutants for *F. fujikuroi DIM5* (H3K9 methyltransferase) and *HP1* (H3K9me3 reading) (Reyes-Dominguez *et al*. 2010; Tamaru and Selker 2001) could be generated, suggesting that the depletion of this mark may result in a lethal phenotype in this fungus (L. Studt, S. M. Rösler and B. Tudzynski, unpublished results). However, it remains to be elucidated whether *A. nidulans* KdmA (Gacek-Matthews *et al*. 2015) and *F. fujikuroi* Kdm4 also antagonize H3K9me3.

In summary, we established distinct and specific roles for the two H3K36 methyltransferases Set2 and Ash1 in *F. fujikuroi*, enzymes which deposit H3K36me3 within euchromatic and subtelomeric regions, respectively. Ash1 was characterized for the first time in a filamentous fungus and was shown to antagonize the heterochromatic mark H3K27me3 at subtelomeric regions. Ash1 is involved in the maintenance of genome stability, likely through direct or indirect recruitment of the DNA repair machinery. ChIP-Seq analysis of other filamentous fungi will show whether the ubiquitous presence of the H3K36 methylation mark along chromosomes is generally conserved in the fungal kingdom. Furthermore, we demonstrated that deletion of both methyltransferase genes, *SET2* and *ASH1*, has an impact on vital cellular processes as well as fungal SM biosynthesis.

## Acknowledgments

We thank Martijn Rep and Petra M. Houterman for their support with the CHEF gel analysis. Furthermore, we are grateful to Shay Covo for critical discussion and to Brian Williamson for critical reading of the manuscript. This work was supported by the German Research Foundation (project number TU101/16-2).

## References


Adhvaryu, K. K., S. A. Morris, B. D. Strahl and E. U. Selker, 2005 Methylation of histone H3 lysine 36 is required for normal development in *Neurospora crassa*. Eukaryot Cell **4:** 1455-1464.

Allis, C. D., S. L. Berger, J. Cote, S. Dent, T. Jenuwien *et al*, 2007 New nomenclature for chromatin-modifying enzymes. Cell **131:** 633-636.

Ausubel, F. M., R. Brent, R. E. Kingston, D. D. Moore, J. G. Seidman *et al*, 1987 *Current protocols in molecular biology*. Wiley, New York.

Bannister, A. J., R. Schneider, F. A. Myers, A. W. Thorne, C. Crane-Robinson *et al*, 2005 Spatial distribution of di- and tri-methyl lysine 36 of histone H3 at active genes. J. Biol. Chem. **280:** 17732-17736.

Barski, A., S. Cuddapah, K. Cui, T. Roh, D. E. Schones *et al*, 2007 High-resolution profiling of histone methylations in the human genome. Cell **129:** 823-837.

Bell, O., C. Wirbelauer, M. Hild, A. N. D. Scharf, M. Schwaiger *et al*, 2007 Localized H3K36 methylation states define histone H4K16 acetylation during transcriptional elongation in *Drosophila*. EMBO J. **26:** 4974-4984.

Bömke, C., and B. Tudzynski, 2009 Diversity, regulation, and evolution of the gibberellin biosynthetic pathway in fungi compared to plants and bacteria. Phytochemistry **70:** 1876-1893.

Brosch, G., P. Loidl and S. Graessle, 2008 Histone modifications and chromatin dynamics: A focus on filamentous fungi. FEMS Microbiol. Rev. **32:** 409-439.

Carrozza, M. J., B. Li, L. Florens, T. Suganuma, S. K. Swanson *et al*, 2005 Histone H3 methylation by Set2 directs deacetylation of coding regions by Rpd3S to suppress spurious intragenic transcription. Cell **123:** 581-592.

Cenis, J. L., 1992 Rapid extraction of fungal DNA for PCR amplification. Nucleic Acids Res. **20:** 2380.

Christianson, T. W., R. S. Sikorski, M. Dante, J. H. Shero and P. Hieter, 1992 Multifunctional yeast high-copy-number shuttle vectors. Gene **110:** 119-122.

Colot, H. V., G. Park, G. E. Turner, C. Ringelberg, C. M. Crew *et al*, 2006 A high-throughput gene knockout procedure for *Neurospora* reveals functions for multiple transcription factors. Proc. Natl. Acad. Sci. U. S. A. **103:** 10352-10357.

Connolly, L. R., K. M. Smith and M. Freitag, 2013 The *Fusarium graminearum* histone H3 K27 methyltransferase KMT6 regulates development and expression of secondary metabolite gene clusters. PLoS Genet. **9:** e1003919.

Darken, M. A., A. L. Jensen and P. Ahu, 1959 Production of gibberellic acid by fermentation. Appl. Microbiol. **7:** 301-303.

Duns, G., E. D. van Berg, I. van Duivenbode, J. Osinga, H. Hollema *et al*, 2010 Histone methyltransferase gene *SETD2* is a novel tumor suppressor gene in clear cell renal cell carcinoma. Cancer Res. **70:** 4287-4291.

Fnu, S., E. A. Williamson, L. P. De Haro, M. Brenneman, J. Wray *et al*, 2011 Methylation of histone H3 lysine 36 enhances DNA repair by nonhomologous end-joining. Proc. Natl. Acad. Sci. U. S. A. **108:** 540-545.

Fox, E. M., and B. J. Howlett, 2008 Secondary metabolism: Regulation and role in fungal biology. Curr. Opin. Microbiol. **11:** 481-487.

Gacek-Matthews, A., L. M. Noble, C. Gruber, H. Berger, M. Sulyok *et al*, 2015 KdmA, a histone H3 demethylase with bipartite function, differentially regulates primary and secondary metabolism in *Aspergillus nidulans*. Mol. Microbiol. **96:** 839-860.

Gao, Y., X. Yan, A. Song, Y. Chang, X. Gao *et al*, 2006 Structural insights into the specific binding of huntingtin proline-rich region with the SH3 and WW domains. Structure **14:** 1755-1765.

Geissman, T. A., A. J. Verbiscar, B. O. Phinney and G. Cragg, 1966 Studies on the biosynthesis of gibberellins from (-)-kaurenoic acid in cultures of *Gibberella fujikuroi*. Phytochemistry **5:** 933-947.

Gu, Q., Z. Wang, X. Sun, T. Ji, H. Huang *et al*, 2017 FvSet2 regulates fungal growth, pathogenicity, and secondary metabolism in *Fusarium verticillioides*. Fungal Genet. Biol. **107:** 24-30.

Hebenstreit, D., M. Gu, S. Haider, D. J. Turner, P. Lió *et al*, 2011 EpiChIP: Gene-by-gene quantification of epigenetic modification levels. Nucleic Acids Res. **39:** e27.

Heimel, K., M. Scherer, M. Vranes, R. Wahl, C. Pothiratana *et al*, 2010 The transcription factor Rbf1 is the master regulator for b-mating type controlled pathogenic development in *Ustilago maydis*. PLoS Pathog. **6:** 17-18.

Janevska, S., B. Arndt, L. Baumann, L. H. Apken, L. M. M. Marques *et al*, 2017 Establishment of the inducible Tet-on system for the activation of the silent trichosetin gene cluster in *Fusarium fujikuroi*. Toxins **9:** 126.

Janevska, S., B. Arndt, E. Niehaus, I. Burkhardt, S. M. Rösler *et al*, 2016 Gibepyrone biosynthesis in the rice pathogen *Fusarium fujikuroi* is facilitated by a small polyketide synthase gene cluster. J. Biol. Chem. **291:** 27403-27420.

Keogh, M., S. K. Kurdistani, S. A. Morris, S. H. Ahn, V. Podolny *et al*, 2005 Cotranscriptional Set2 methylation of histone H3 lysine 36 recruits a repressive Rpd3 complex. Cell **123:** 593-605.

Kim, T., and S. Buratowski, 2007 Two *Saccharomyces cerevisiae* JmjC domain proteins demethylate histone H3 Lys36 in transcribed regions to promote elongation. J. Biol. Chem. **282:** 20827-20835.

Kizer, K. O., H. P. Phatnani, Y. Shibata, H. Hall, A. L. Greenleaf *et al*, 2005 A novel domain in Set2 mediates RNA polymerase II interaction and couples histone H3 K36 methylation with transcript elongation. Mol. Cell. Biol. **25:** 3305-3316.

Klose, R. J., K. E. Gardner, G. Liang, H. Erdjument-Bromage, P. Tempst *et al*, 2007 Demethylation of histone H3K36 and H3K9 by Rph1: A vestige of an H3K9 methylation system in *Saccharomyces cerevisiae*? Mol. Cell. Biol. **27:** 3951-3961.

Klose, R. J., K. Yamane, Y. Bae, D. Zhang, H. Erdjument-Bromage *et al*, 2006 The transcriptional repressor JHDM3A demethylates trimethyl histone H3 lysine 9 and lysine 36. Nature **442:** 312-316.

Krogan, N. J., M. Kim, A. Tong, A. Golshani, G. Cagney *et al*, 2003 Methylation of histone H3 by Set2 in *Saccharomyces cerevisiae* is linked to transcriptional elongation by RNA polymerase II. Mol. Cell. Biol. **23:** 4207-4218.

Laemmli, U. K., 1970 Cleavage of structural proteins during the assembly of the head of bacteriophage T4. Nature **227:** 680-685.

Leslie, J. F., and B. A. Summerell, 2006 *Fusarium* laboratory workshops - A recent history. Mycotoxin Research **22:** 73-74.

Li, F., G. Mao, D. Tong, J. Huang, L. Gu *et al*, 2013 The histone mark H3K36me3 regulates human DNA mismatch repair through its interaction with MutSα. Cell **153:** 590-600.

Li, M., H. P. Phatnani, Z. Guan, H. Sage, A. L. Greenleaf *et al*, 2005 Solution structure of the Set2-Rpb1 interacting domain of human Set2 and its interaction with the hyperphosphorylated C-terminal domain of Rpb1. Proc. Natl. Acad. Sci. U. S. A. **102:** 17636-17641.

Liu, Y., N. Liu, Y. Yin, Y. Chen, J. Jiang *et al*, 2015 Histone H3K4 methylation regulates hyphal growth, secondary metabolism and multiple stress responses in *Fusarium graminearum*. Environ. Microbiol. **17:** 4615-4630.

Livak, K. J., and T. D. Schmittgen, 2001 Analysis of relative gene expression data using real-time quantitative PCR and the 2-ΔΔCT method. Methods **25:** 402-408.

Lu, T., M. W. Jackson, B. Wang, M. Yang, M. R. Chance *et al*, 2010 Regulation of NF-κB by NSD1/FBXL11-dependent reversible lysine methylation of p65. Proc. Natl. Acad. Sci. U. S. A. **107:** 46-51.

Lundblad, V., 2001 Genome instability: McClintock revisited. Curr. Biol. **11:** R957-R960.

Miao, F., and R. Natarajan, 2005 Mapping global histone methylation patterns in the coding regions of human genes. Mol. Cell. Biol. **25:** 4650-4661.

Michielse, C. B., L. Studt, S. Janevska, C. M. K. Sieber, B. Arndt *et al*, 2015 The global regulator FfSge1 is required for expression of secondary metabolite gene clusters but not for pathogenicity in *Fusarium fujikuroi*. Environ. Microbiol. **17:** 2690-2708.

930 Ng, H. H., F. Robert, R. A. Young and K. Struhl, 2003 Targeted recruitment of Set1 histone
931 methylase by elongating pol II provides a localized mark and memory of recent
932 transcriptional activity. Mol. Cell **11:** 709-719.

933 Niehaus, E., K. W. von Bargen, J. J. Espino, A. Pfannmüller, H. Humpf *et al*, 2014
934 Characterization of the fusaric acid gene cluster in *Fusarium fujikuroi*. Appl. Microbiol.
935 Biotechnol. **98:** 1749-1762.

936 Niehaus, E., K. Kleigrewe, P. Wiemann, L. Studt, C. M. K. Sieber *et al*, 2013 Genetic
937 manipulation of the *Fusarium fujikuroi* fusarin gene cluster yields insight into the complex
938 regulation and fusarin biosynthetic pathway. Chem. Biol. **20:** 1055-1066.

939 Nirenberg, H. I., and K. O'Donnell, 1998 New *Fusarium* species and combinations within the
940 *Gibberella fujikuroi* species complex. Mycologia **90:** 434-458.

941 Pfaffl, M. W., 2001 A new mathematical model for relative quantification in real-time RT-
942 PCR. Nucleic Acids Res. **29:** e45.

943 Pfister, S., S. Ahrabi, L. Zalmas, S. Sarkar, F. Aymard *et al*, 2014 SETD2-dependent histone
944 H3K36 trimethylation is required for homologous recombination repair and genome stability.
945 Cell Rep. **7:** 2006-2018.

946 Pokholok, D. K., C. T. Harbison, S. Levine, M. Cole, N. M. Hannett *et al*, 2005 Genome-wide
947 map of nucleosome acetylation and methylation in yeast. Cell **122:** 517-527.

948 Pontecorvo, G., J. A. Roper, L. M. Chemmons, K. D. Macdonald and A. W. J. Bufton, 1953
949 The genetics of *Aspergillus nidulans*. Adv. Genet. **5:** 141-238.

950 Rando, O. J., and H. Y. Chang, 2009 Genome-wide views of chromatin structure. Annu. Rev.
951 Biochem. **78:** 245-271.

952 Reyes-Dominguez, Y., J. W. Bok, H. Berger, E. K. Shwab, A. Basheer *et al*, 2010
953 Heterochromatic marks are associated with the repression of secondary metabolism clusters in
954 *Aspergillus nidulans*. Mol. Microbiol. **76:** 1376-1386.

955 Rösler, S. M., K. Kramer, I. Finkemeier, H. Humpf and B. Tudzynski, 2016 The SAGA
956 complex in the rice pathogen *Fusarium fujikuroi*: Structure and functional characterization.
957 Mol. Microbiol. **102:** 951-974.

958 Sambrook, J., E. F. Fritsch and T. Maniatis, 1989 *Molecular cloning: A laboratory manual*.
959 Cold Spring Harbor, New York.

960 Santos-Rosa, H., R. Schneider, A. J. Bannister, J. Sherriff, B. E. Bernstein *et al*, 2002 Active
961 genes are tri-methylated at K4 of histone H3. Nature **419:** 407-411.

962 Schotanus, K., J. L. Soyer, L. R. Connolly, J. Grandaubert, P. Happel *et al*, 2015 Histone
963 modifications rather than the novel regional centromeres of *Zymoseptoria tritici* distinguish
964 core and accessory chromosomes. Epigenetics Chromatin **8:** 41.

965 Schumacher, J., 2012 Tools for *Botrytis cinerea*: New expression vectors make the gray mold
966 fungus more accessible to cell biology approaches. Fungal Genet. Biol. **49:** 483-497.

Schwämmle, V., C. Aspalter, S. Sidoli and O. N. Jensen, 2014 Large scale analysis of co-existing post-translational modifications in histone tails reveals global fine structure of cross-talk. Mol. Cell. Proteomics **13:** 1855-1865.

Southern, E. M., 1975 Detection of specific sequences among DNA fragments separated by gel electrophoresis. J. Mol. Biol. **98:** 503-517.

Staben, C., B. Jensen, M. Singer, J. Pollock, M. Schechtmann *et al*, 1989 Use of a bacterial hygromycin B resistance gene as a dominant selectable marker in *Neurospora crassa* transformation. Fungal Genet. Newslett. **36:** 79-81.

Strahl, B. D., P. A. Grant, S. D. Briggs, Z. Sun, J. R. Bone *et al*, 2002 Set2 is a nucleosomal histone H3-selective methyltransferase that mediates transcriptional repression. Mol. Cell. Biol. **22:** 1298-1306.

Studt, L., P. Wiemann, K. Kleigrewe, H. Humpf and B. Tudzynski, 2012 Biosynthesis of fusarubins accounts for pigmentation of *Fusarium fujikuroi* perithecia. Appl. Environ. Microbiol. **78:** 4468-4480.

Studt, L., S. Janevska, B. Arndt, S. Boedi, M. Sulyok *et al*, 2017 Lack of the COMPASS component Ccl1 reduces H3K4 trimethylation levels and affects transcription of secondary metabolite genes in two plant-pathogenic *Fusarium* species. Front. Microbiol. **7:** 2144.

Studt, L., S. M. Rösler, I. Burkhardt, B. Arndt, M. Freitag *et al*, 2016a Knock-down of the methyltransferase Kmt6 relieves H3K27me3 and results in induction of cryptic and otherwise silent secondary metabolite gene clusters in *Fusarium fujikuroi*. Environ. Microbiol. **18:** 4037-4054.

Studt, L., S. Janevska, E. Niehaus, I. Burkhardt, B. Arndt *et al*, 2016b Two separate key enzymes and two pathway-specific transcription factors are involved in fusaric acid biosynthesis in *Fusarium fujikuroi*. Environ Microbiol **18:** 936-956.

Sun, S., and W. C. Snyder, 1981 The *bakanae* disease of the rice plant, pp. 104-113 in *Fusarium: Diseases, Biology and Taxonomy*, edited by P. E. Nelson, T. A. Toussoun and R. J. Cook. The Pennsylvania State University Press, University Park.

Sun, X., J. Wei, X. Wu, M. Hu, L. Wang *et al*, 2005 Identification and characterization of a novel human histone H3 lysine 36-specific methyltransferase. J. Biol. Chem. **280:** 35261-35271.

Tamaru, H., and E. U. Selker, 2001 A histone H3 methyltransferase controls DNA methylation in *Neurospora crassa*. Nature **414:** 277-283.

Tanaka, Y., Z. Katagiri, K. Kawahashi, D. Kioussis and S. Kitajima, 2007 Trithorax-group protein ASH1 methylates histone H3 lysine 36. Gene **397:** 161-168.

Teunissen, H. A. S., J. Verkooijen, B. J. C. Cornelissen and M. A. Haring, 2002 Genetic exchange of avirulence determinants and extensive karyotype rearrangements in parasexual recombinants of *Fusarium oxysporum*. Mol. Genet. Genomics **268:** 298-310.

Tsukada, Y., J. Fang, H. Erdjument-Bromage, M. E. Warren, C. H. Borchers *et al*, 2006 Histone demethylation by a family of JmjC domain-containing proteins. Nature **439:** 811-816.

Tudzynski, B., and K. Hölter, 1998 Gibberellin biosynthetic pathway in *Gibberella fujikuroi*: Evidence for a gene cluster. Fungal Genet. Biol. **25:** 157-170.

Tudzynski, B., V. Homann, B. Feng and G. A. Marzluf, 1999 Isolation, characterization and disruption of the *areA* nitrogen regulatory gene of *Gibberella fujikuroi*. Mol. Gen. Genet. **261:** 106-114.

Tyanova, S., T. Temu, P. Sinitcyn, A. Carlson, M. Y. Hein *et al*, 2016 The Perseus computational platform for comprehensive analysis of (prote)omics data. Nat. Methods **13:** 731-740.

Vakoc, C. R., M. M. Sachdeva, H. Wang and G. A. Blobel, 2006 Profile of histone lysine methylation across transcribed mammalian chromatin. Mol. Cell. Biol. **26:** 9185-9195.

Venkatesh, S., and J. L. Workman, 2013 Set2 mediated H3 lysine 36 methylation: Regulation of transcription elongation and implications in organismal development. Wiley Interdiscip. Rev. Dev. Biol. **2:** 685-700.

Wagner, E. J., and P. B. Carpenter, 2012 Understanding the language of Lys36 methylation at histone H3. Nat. Rev. Mol. Cell Biol. **13:** 115-126.

Wang, C. I., A. A. Alekseyenko, G. Leroy, A. E. H. Elia, A. A. Gorchakov *et al*, 2013 Chromatin proteins captured by ChIP-mass spectrometry are linked to dosage compensation in *Drosophila*. Nat. Struct. Mol. Biol. **20:** 202-209.

Wiemann, P., A. Willmann, M. Straeten, K. Kleigrewe, M. Beyer *et al*, 2009 Biosynthesis of the red pigment bikaverin in *Fusarium fujikuroi*: Genes, their function and regulation. Mol. Microbiol. **72:** 931-946.

Wiemann, P., S. Albermann, E. Niehaus, L. Studt, K. W. von Bargen *et al*, 2012 The Sfp-type 4′-phosphopantetheinyl transferase Ppt1 of *Fusarium fujikuroi* controls development, secondary metabolism and pathogenicity. PLoS ONE **7:** e37519.

Wiemann, P., C. M. K. Sieber, K. W. von Bargen, L. Studt, E. Niehaus *et al*, 2013 Deciphering the cryptic genome: Genome-wide analyses of the rice pathogen *Fusarium fujikuroi* reveal complex regulation of secondary metabolism and novel metabolites. PLoS Pathog. **9:** e1003475.

Wiles, E. T., and E. U. Selker, 2017 H3K27 methylation: A promiscuous repressive chromatin mark. Curr. Opin. Genet. Dev. **43:** 31-37.

Winston, F., C. Dollard and S. L. Ricupero-Hovasse, 1995 Construction of a set of convenient *Saccharomyces cerevisiae* strains that are isogenic to S288C. Yeast **11:** 53-55.

Xu, L., Z. Zhao, A. Dong, L. Soubigou-Taconnat, J. Renou *et al*, 2008 Di- and tri- but not monomethylation on histone H3 lysine 36 marks active transcription of genes involved in flowering time regulation and other processes in *Arabidopsis thaliana*. Mol. Cell. Biol. **28:** 1348-1360.

Yuan, W., M. Xu, C. Huang, N. Liu, S. Chen *et al*, 2011 H3K36 methylation antagonizes PRC2-mediated H3K27 methylation. J. Biol. Chem. **286:** 7983-7989.

## Figure legends

**Figure 1. *F. fujikuroi* Set2 and Ash1 are H3K36-specific histone methyltransferases.** A) Schematic representation of the domain structure of *S. cerevisiae* and *F. fujikuroi* Set2 and *F. fujikuroi* Ash1. B) Domain description including the respective InterPro accession numbers. C) and D) Western blot analysis using the H3K36me3, H3K36me2 and H3 antibodies. The wild type (WT) and indicated strains were grown for 3 days in liquid culture (60 mM glutamine) prior to protein extraction. 15 µg of the protein extract was loaded on to the gel for H3K36me3 and H3 antibodies, while 30 µg was loaded for H3K36me2. The relative global amount of H3K36me3 was determined using a photo editing software, and the intensity of the WT band was set to 100%.

**Figure 2. Influence of *SET2* and *ASH1* deletion on vegetative growth.** A) The wild type (WT) as well as two independent mutants of Δ*set2*, Δ*ash1* and *H3K36A* were grown on complex (V8, CM) and minimal (CD) media for 7 days in the dark in triplicates. B) The WT, Δ*set2* T2, Δ*ash1* T2, *H3K36A* T8 and three independent Δ*set2*/Δ*ash1* double mutants were grown under above described conditions.

**Figure 3. H3K36me3 distribution on chromosomes I, X and XII.** The wild type (WT) and Δ*ash1* T2 were grown for 3 days in liquid culture in the presence of limiting (6 mM, N-) and saturating (60 mM, N+) amounts of glutamine prior to ChIP-Seq analysis using the H3K36me3 antibody. The WT and Δ*ash1* input samples were not treated with antibody before sequencing. Shown are A) chromosome I, B) chromosome X and C) chromosome XII as well as the respective SM key genes located on these chromosomes. For the PCR analysis of subtelomere/chromosome stability, six independent Δ*ash1* mutants were analyzed using

gene-specific primers. When several PCRs for the same chromosome arm are shown, "Tel" indicates the use of primers for the outermost gene close to the telomere, while "Cen" indicates the use of primers for the innermost gene close to the centromere. WT DNA and $H_2O$ were used as positive and negative controls, respectively. For each chromosome, control PCRs are shown.

**Figure 4. Microarray expression analysis of differentially regulated genes in Δ*set2* T1 and Δ*ash1* T2.** The wild type (WT) and the two deletion mutants were grown in liquid culture in the presence of limiting (6 mM, N-) and saturating (60 mM, N+) amounts of glutamine (Gln) for 3 days prior to RNA extraction. Data are mean values ($n$ = 2). Differential regulation is shown for A) 6 mM Gln and B) 60 mM Gln. Genes upregulated in the deletion mutants compared to the WT are green ($\log_2$-fold change ≥ 2), downregulated genes are red ($\log_2$-fold change ≤ -2), and not differentially expressed genes are black (between -2 and 2). The eight profiles were extracted first, and then the genes were clustered for each profile.

**Figure 5. Secondary metabolite biosynthesis is deregulated in Δ*set2*, Δ*ash1* and *H3K36A* mutants.** The wild type (WT) and two independent mutants of Δ*set2*, Δ*ash1* and *H3K36A* were grown in liquid culture for 7 days and analyzed *via* HPLC-DAD. The production was related to the dry weight of the strains and the production level of the WT was set to 100%. Data are mean values ± SD ($n$ = 3). For statistical analysis, the mutants were compared with the WT using the student's t-test: *, $p < 0.05$; **, $p < 0.01$. A) The strains were grown in the presence of 6 mM glutamine, the producing condition for bikaverin (BIK). The production of fusarubins (FSR) in the mutants was related to the WT production under FSR-inducing conditions (6 mM $NaNO_3$). B) The strains were grown in the presence of 60 mM glutamine, the producing condition for fusarins (FUS) and fusaric acid (FSA). C) The strains were grown in the presence of 6 mM glutamine, the producing condition for gibberellic acid $GA_3$. n.d., not detected.

**Figure 6. Comparison between H3K36me3 levels and absolute expression at the gibberellic acid (GA) and bikaverin (BIK) clusters, as well as at the *UBI* reference gene.** The wild type (WT) and Δ*ash1* T2 were grown for 3 days in liquid culture in the presence of limiting (6 mM, N-) and saturating (60 mM, N+) amounts of glutamine (Gln) prior to ChIP-Seq analysis using the H3K36me3 antibody. The WT and Δ*ash1* input samples were not treated with antibody before sequencing. Shown are the A) GA cluster, B) BIK cluster and C) *UBI* as well as adjacent regions. Absolute expression profiles are taken from the microarray analysis, and the data are mean values ($n$ = 2).

**Figure 7. H3K36me3 and H3K27me3 levels at the gibberellic acid (GA) and bikaverin (BIK) clusters, as well as at the *UBI* reference gene.** A) The wild type (WT), Δ*set2* T1, Δ*ash1* T2 and *H3K36A* T8 were grown for 3 days in liquid culture prior to ChIP-qRT-PCR using the H3K36me3 antibody. B) The WT and indicated strains were grown for 3 days in liquid culture prior to ChIP-qRT-PCR using the H3K27me3 antibody. The WT grown in the presence of 60 mM glutamine (Gln) was arbitrarily set to 1, and the data are mean values ± SD ($n$ = 4). For statistical analysis, Δ*set2* and Δ*ash1* were compared to the *H3K36A* mutant using the student's t-test: **, $p < 0.01$. Primers binding at the 3' gene ends were applied. For H3K27me3, the use of primers binding at the 5' ends of these genes gave very similar results.

**Figure 8. Pathogenicity on rice of Δ*set2* and Δ*ash1* deletion mutants.** A) Germinated rice seedlings were infected with 100 ppm gibberellic acid $GA_3$ (positive control), $H_2O$ (negative control), the wild type (WT) as well as Δ*set2* T1 and Δ*ash1* T2 deletion mutants for 7 days. Data are mean values ± SD ($n$ = 3). For statistical analysis, the mutants were compared with the WT using the student's t-test: **, $p < 0.01$. B) Four infected rice roots per sample were combined and freeze-dried prior to genomic DNA (gDNA) extraction. Quantification was performed with real-time PCR and the ΔCt method. The ratio of fungal/plant gDNA of the WT-infected roots was set to 100%, and the data are mean values ($n$ = 2).

**Figure 9. Distinct roles of H3K36me3 deposited by Set2 and Ash1 in *F. fujikuroi*.** Set2 deposited H3K36me3 overlaps with euchromatic H3K4me2/me3 and is most likely involved in transcriptional elongation *via* the putative interaction of Set2 with RNA polymerase (Pol) II. In contrast, Ash1 deposited H3K36me3 overlaps with H3K27me3 of facultative heterochromatin. Our data suggest that it exerts a role in the repair of DNA double strand breaks, likely counteracting H3K27 methylation. H3K9me3 most likely makes up the constitutive heterochromatin of *F. fujikuroi* centromeres.

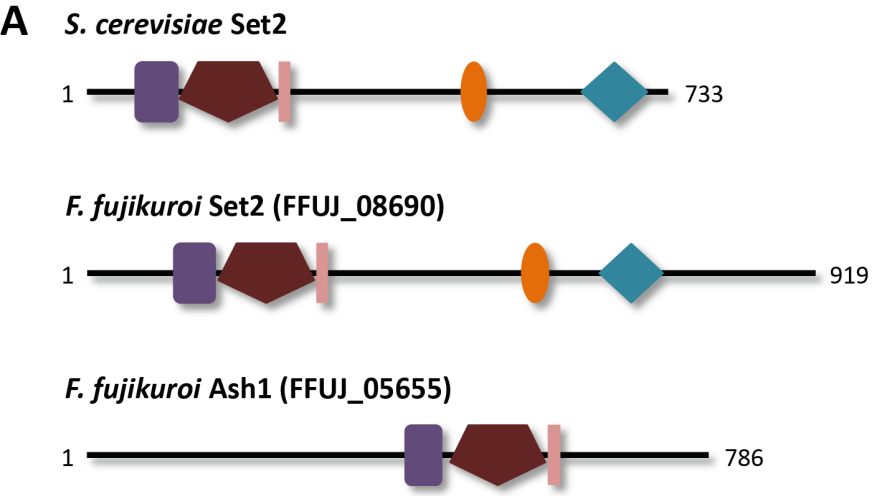


B

| Symbol | Domain description |
|---|---|
| | IPR001214 Su(var)3-9, Enhancer-of-zeste, Trithorax (SET) domain |
| | IPR006560 Associated with SET (AWS) |
| | IPR003616 Post-SET domain |
| | IPR001202 WW/Rsp5/WWP |
| | IPR013257 Set2 Rpb1 interacting (SRI) |

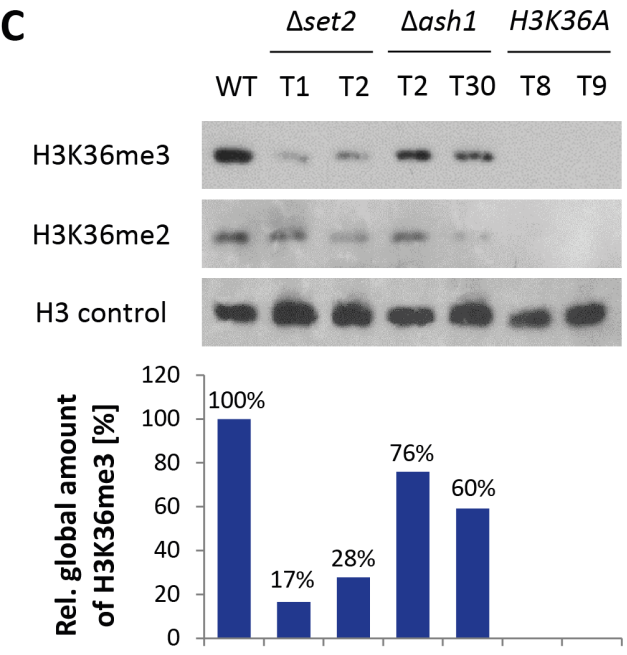


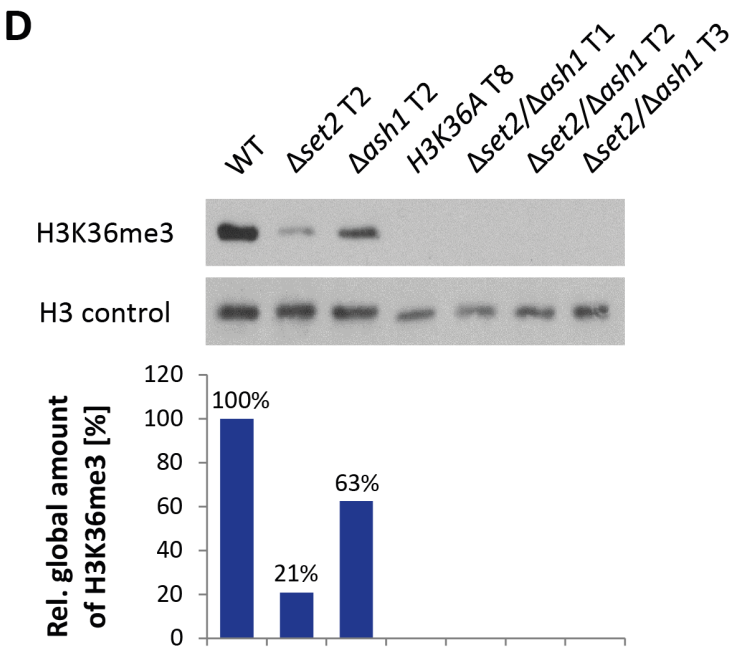

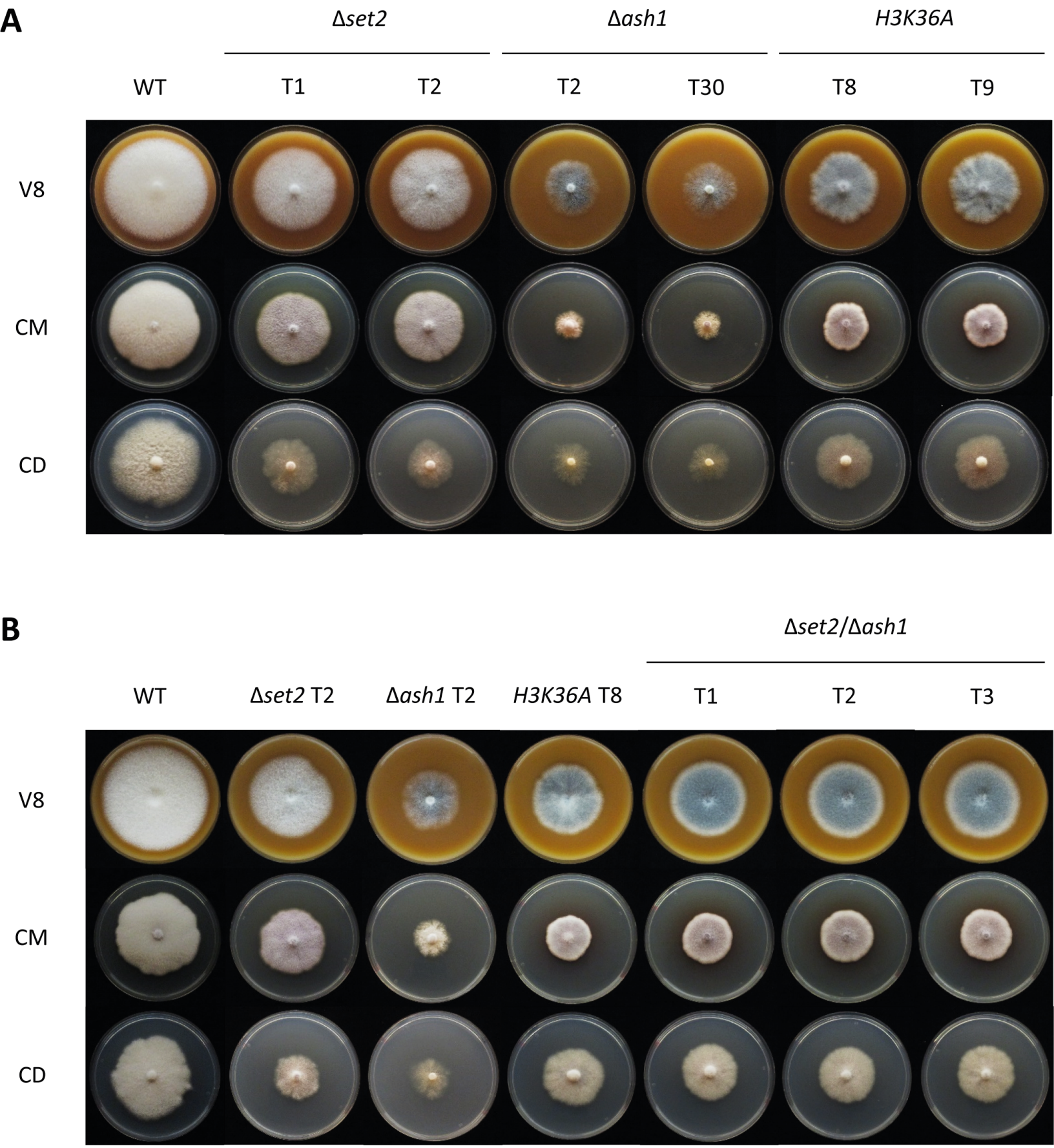
A
Δset2
Δash1
H3K36A
WT
T1
T2
T2
T30
T8
T9
V8
CM
CD
B
Δset2/Δash1
WT
Δset2 T2
Δash1 T2
H3K36A T8
T1
T2
T3
V8
CM
CD

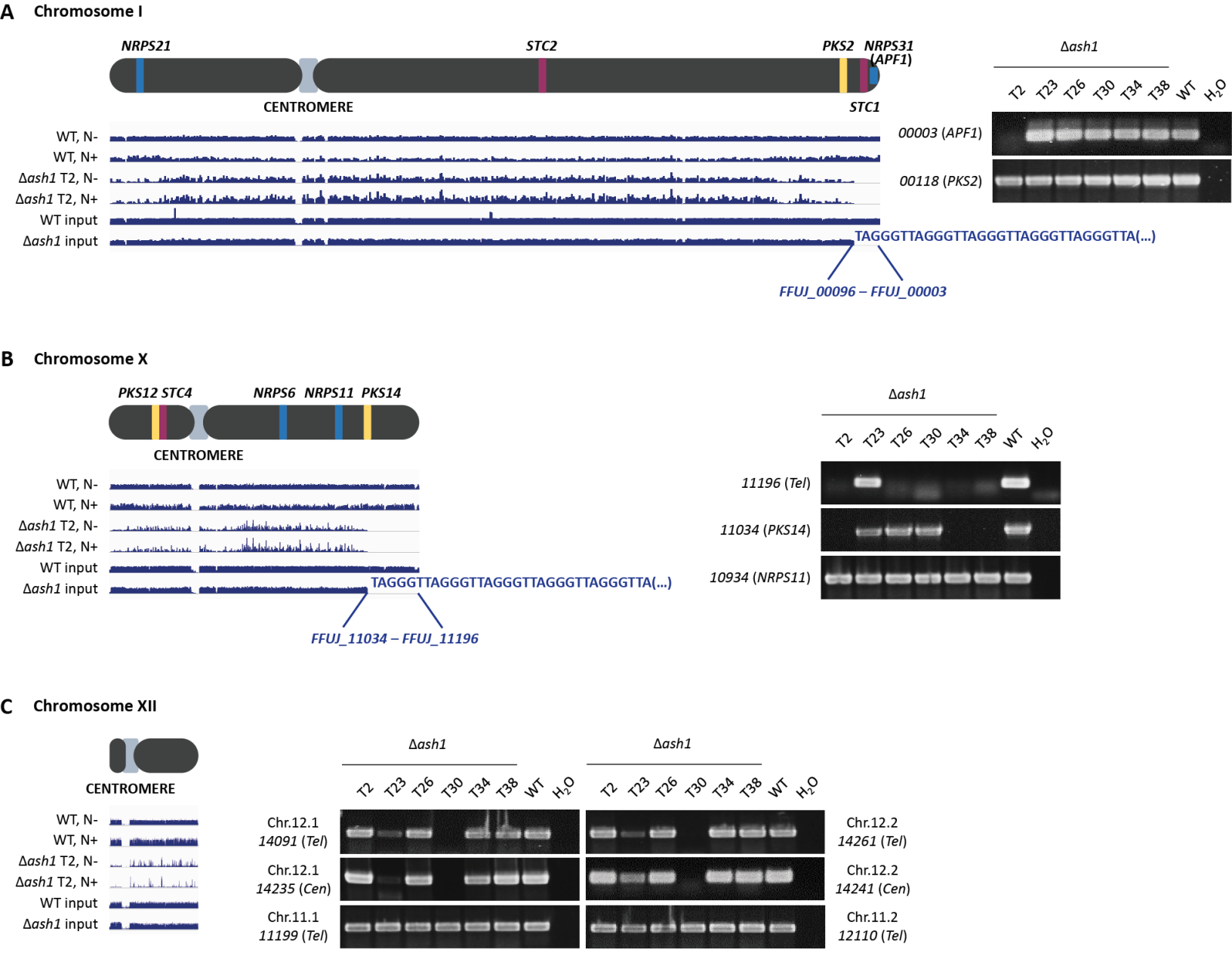
A
Chromosome I
NRPS21
STC2
PKS2
NRPS31 (APF1)
CENTROMERE
STC1
WT, N-
WT, N+
Δash1 T2, N-
Δash1 T2, N+
WT input
Δash1 input
TAGGGTTAGGGTTAGGGTTAGGGTTAGGGTTA(...)
FFUJ_00096 – FFUJ_00003
Δash1
T2 T23 T26 T30 T34 T38 WT H2O
00003 (APF1)
00118 (PKS2)
B
Chromosome X
PKS12 STC4
NRPS6 NRPS11 PKS14
CENTROMERE
WT, N-
WT, N+
Δash1 T2, N-
Δash1 T2, N+
WT input
Δash1 input
TAGGGTTAGGGTTAGGGTTAGGGTTAGGGTTA(...)
FFUJ_11034 – FFUJ_11196
Δash1
T2 T23 T26 T30 T34 T38 WT H2O
11196 (Tel)
11034 (PKS14)
10934 (NRPS11)
C
Chromosome XII
CENTROMERE
WT, N-
WT, N+
Δash1 T2, N-
Δash1 T2, N+
WT input
Δash1 input
Δash1
Δash1
T2 T23 T26 T30 T34 T38 WT H2O
T2 T23 T26 T30 T34 T38 WT H2O
Chr.12.1 14091 (Tel)
Chr.12.1 14235 (Cen)
Chr.11.1 11199 (Tel)
Chr.12.2 14261 (Tel)
Chr.12.2 14241 (Cen)
Chr.11.2 12110 (Tel)

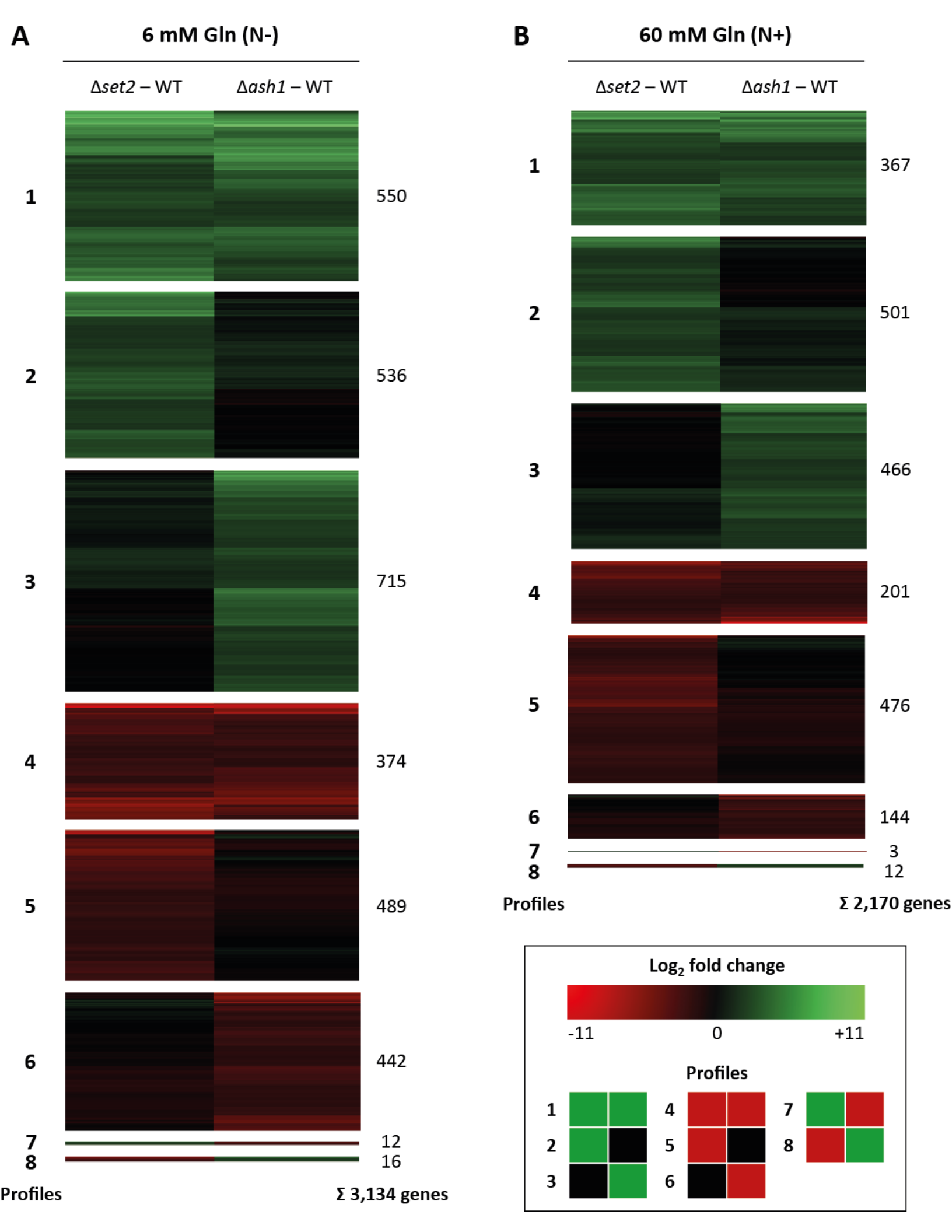
A
6 mM Gln (N-)
Δset2 – WT
Δash1 – WT
1
550
2
536
3
715
4
374
5
489
6
442
7
12
8
16
Profiles
Σ 3,134 genes
B
60 mM Gln (N+)
Δset2 – WT
Δash1 – WT
1
367
2
501
3
466
4
201
5
476
6
144
7
3
8
12
Profiles
Σ 2,170 genes
Log2 fold change
-11
0
+11
Profiles
1
2
3
4
5
6
7
8

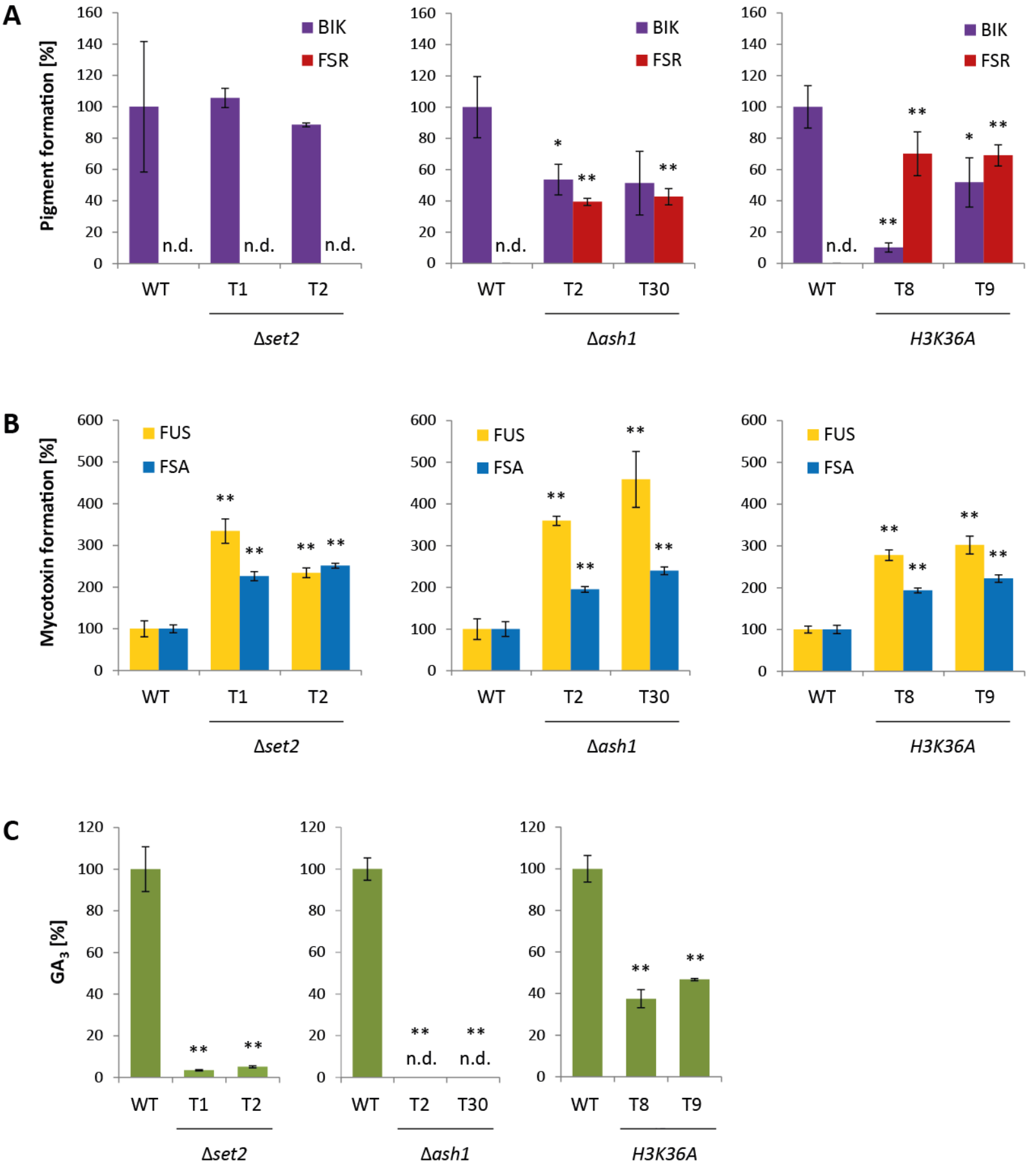
A
Pigment formation [%]
BIK
FSR
n.d.
WT
T1
T2
Δset2
T30
Δash1
T8
T9
H3K36A
B
Mycotoxin formation [%]
FUS
FSA
C
GA3 [%]

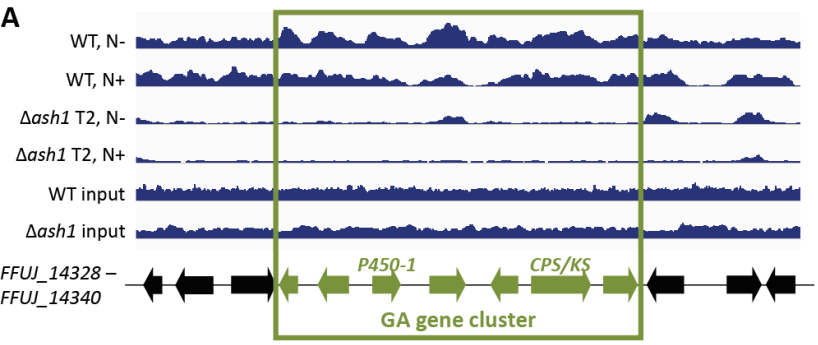
A
WT, N-
WT, N+
Δash1 T2, N-
Δash1 T2, N+
WT input
Δash1 input
FFUJ_14328 –
FFUJ_14340
P450-1
CPS/KS
GA gene cluster

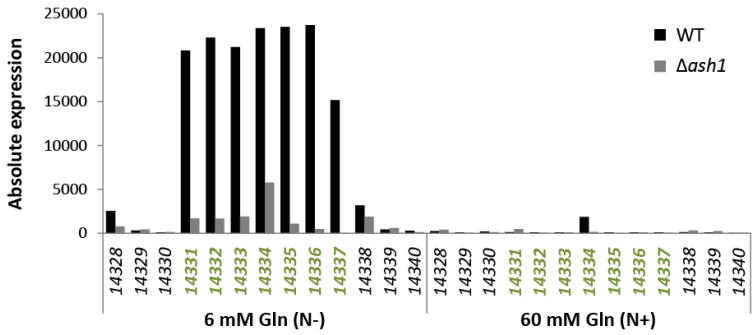
Absolute expression
25000
20000
15000
10000
5000
0
WT
Δash1
14328 14329 14330 14331 14332 14333 14334 14335 14336 14337 14338 14339 14340
14328 14329 14330 14331 14332 14333 14334 14335 14336 14337 14338 14339 14340
6 mM Gln (N-)
60 mM Gln (N+)

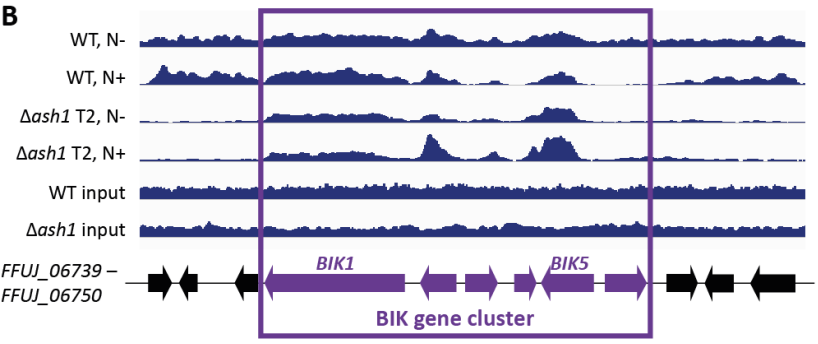
B
WT, N-
WT, N+
Δash1 T2, N-
Δash1 T2, N+
WT input
Δash1 input
FFUJ_06739 –
FFUJ_06750
BIK1
BIK5
BIK gene cluster

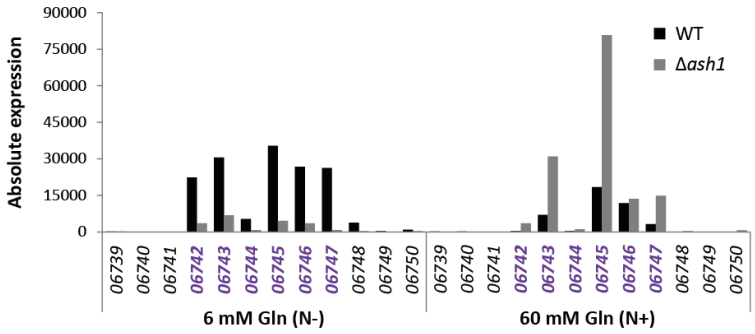
Absolute expression
90000
75000
60000
45000
30000
15000
0
WT
Δash1
06739 06740 06741 06742 06743 06744 06745 06746 06747 06748 06749 06750
06739 06740 06741 06742 06743 06744 06745 06746 06747 06748 06749 06750
6 mM Gln (N-)
60 mM Gln (N+)

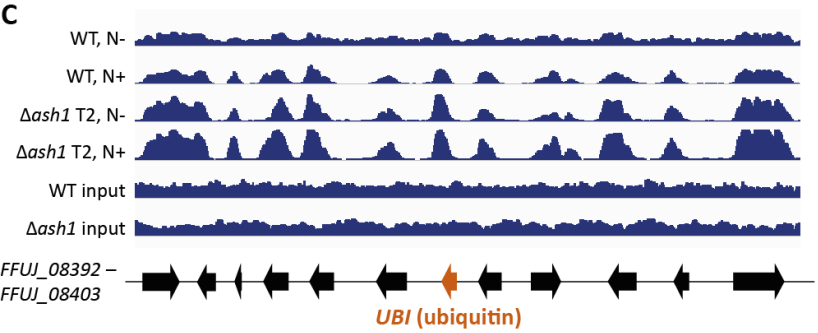
C
WT, N-
WT, N+
Δash1 T2, N-
Δash1 T2, N+
WT input
Δash1 input
FFUJ_08392 –
FFUJ_08403
UBI (ubiquitin)

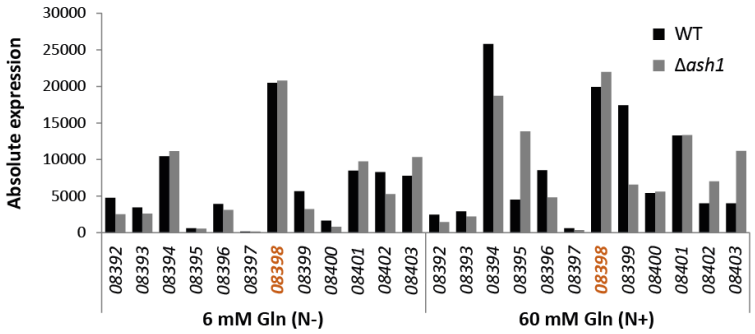
Absolute expression
30000
25000
20000
15000
10000
5000
0
WT
Δash1
08392 08393 08394 08395 08396 08397 08398 08399 08400 08401 08402 08403
08392 08393 08394 08395 08396 08397 08398 08399 08400 08401 08402 08403
6 mM Gln (N-)
60 mM Gln (N+)

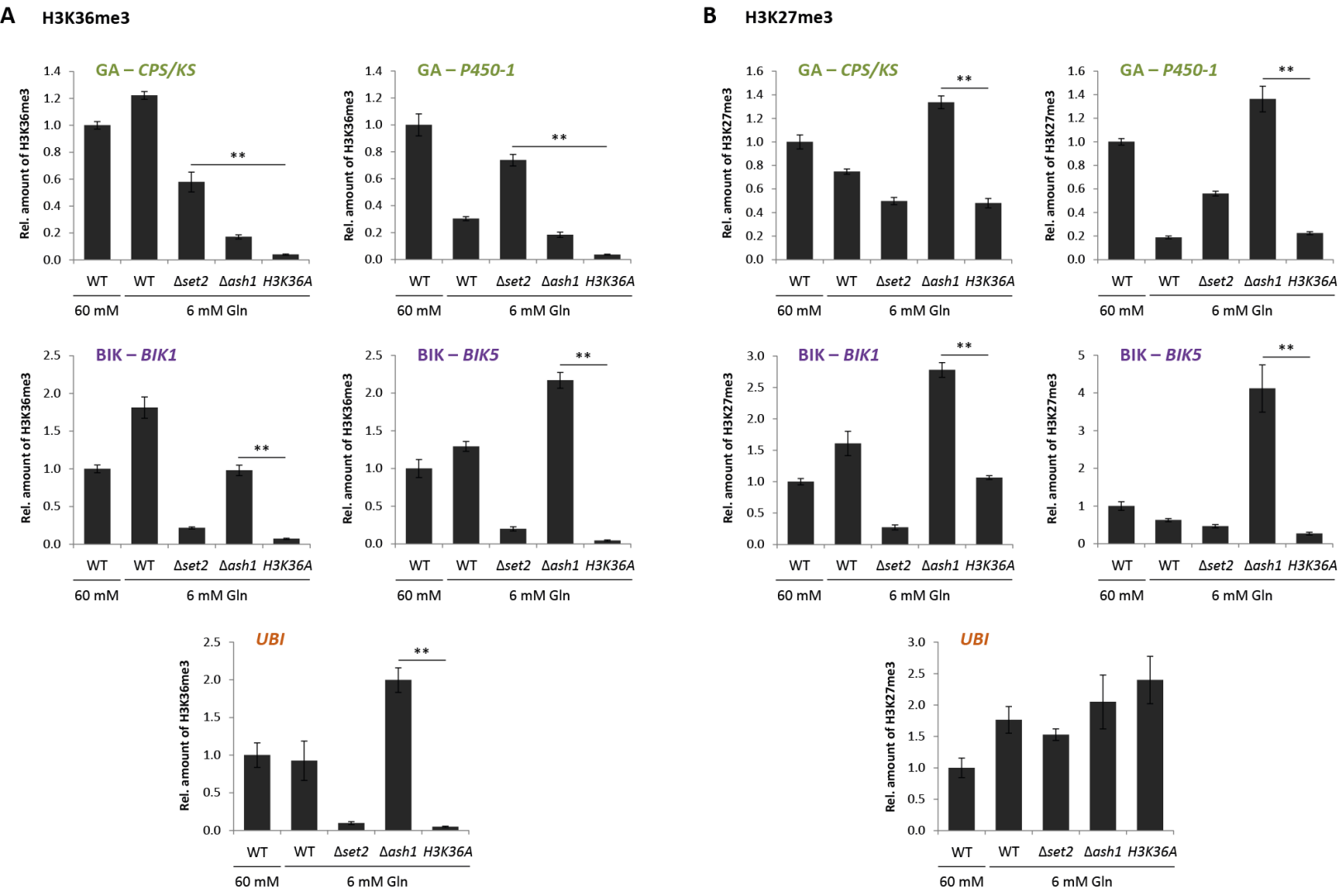
A
H3K36me3
GA – CPS/KS
GA – P450-1
BIK – BIK1
BIK – BIK5
UBI
Rel. amount of H3K36me3
WT
WT
Δset2
Δash1
H3K36A
60 mM
6 mM Gln
**
B
H3K27me3
Rel. amount of H3K27me3

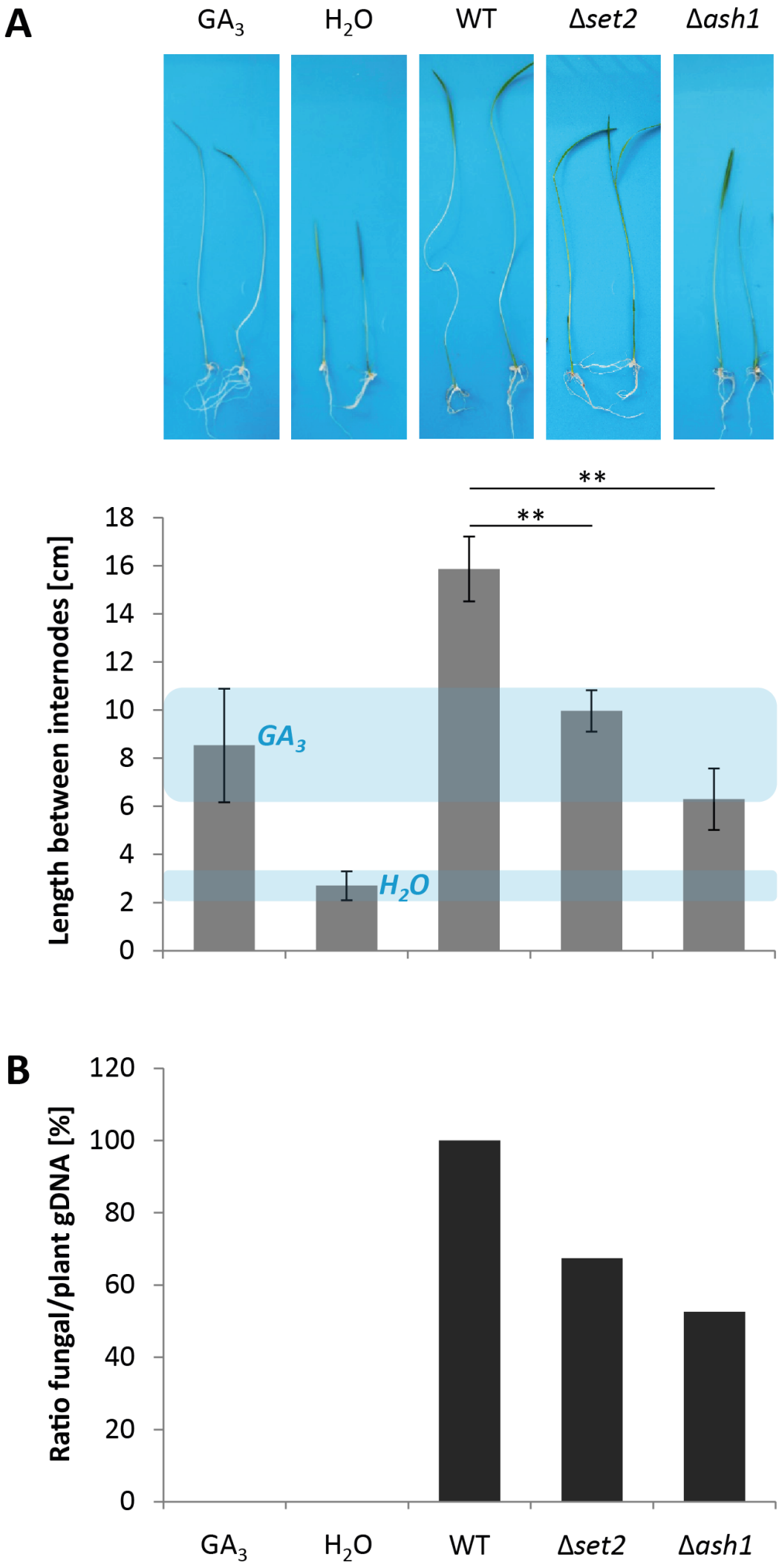
A
GA3
H2O
WT
Δset2
Δash1
**
**
Length between internodes [cm]
18
16
14
12
10
8
6
4
2
0
GA3
H2O
B
Ratio fungal/plant gDNA [%]
120
100
80
60
40
20
0
GA3
H2O
WT
Δset2
Δash1

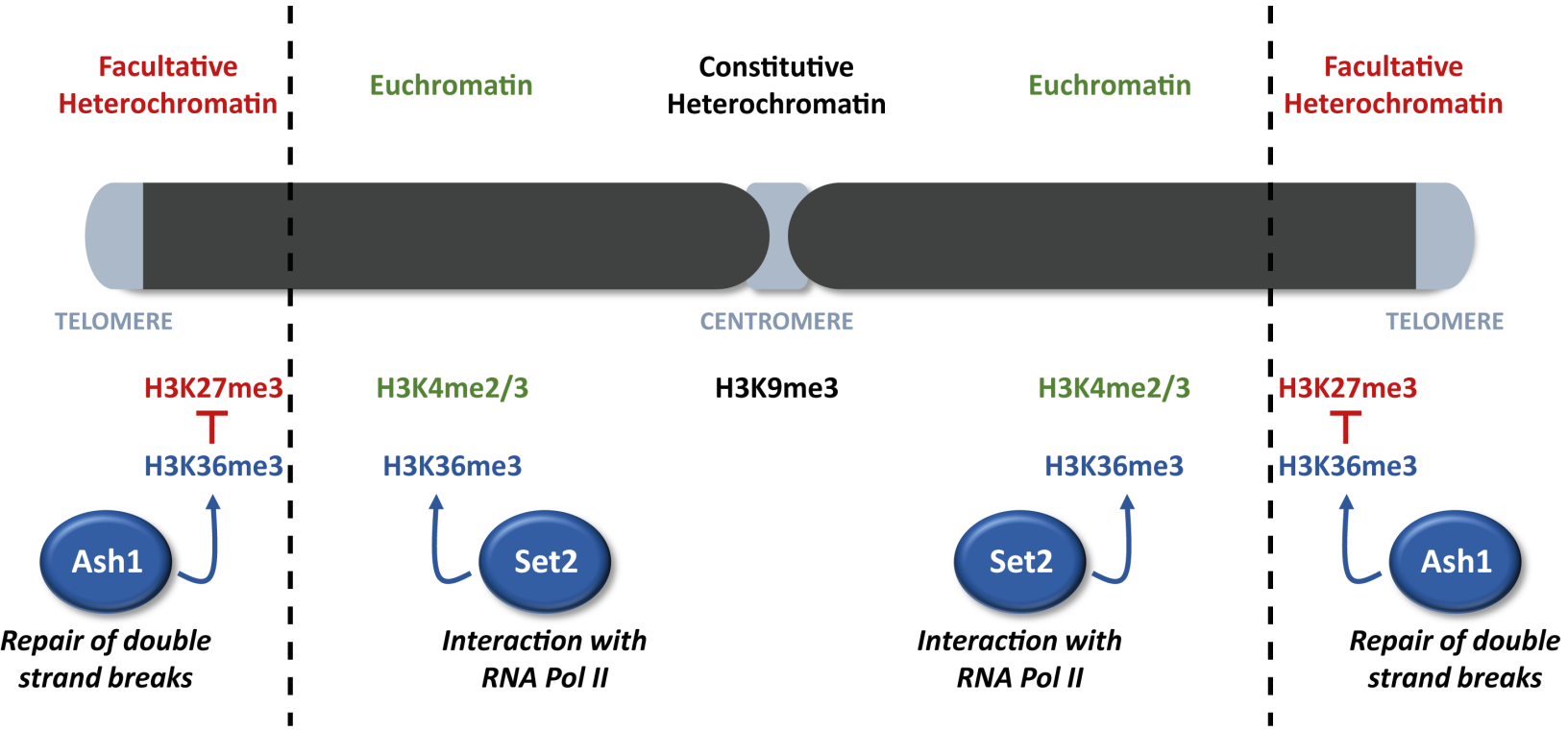
Facultative Heterochromatin
Euchromatin
Constitutive Heterochromatin
Euchromatin
Facultative Heterochromatin
TELOMERE
CENTROMERE
TELOMERE
H3K27me3
H3K36me3
H3K4me2/3
H3K36me3
H3K9me3
H3K4me2/3
H3K36me3
H3K27me3
H3K36me3
Ash1
Set2
Set2
Ash1
Repair of double strand breaks
Interaction with RNA Pol II
Interaction with RNA Pol II
Repair of double strand breaks